GEORGIA DOT RESEARCH PROJECT 18-07

Final Report

BEST PRACTICES AND SPECIFICATIONS FOR MASSIVE CONCRETE DRILLED SHAFTS

Office of Performance-based Management and Research
600 West Peachtree NW | Atlanta, GA 30308

February 2022

TECHNICAL REPORT DOCUMENTATION PAGE

1. Report No.: FHWA-GA-22-1807	2. Government Accession No.: N/A	3. Recipient's Catalog No.: N/A	
4. Title and Subtitle: Best Practices and Specifications for Massive Concrete Drilled Shafts		5. Report Date: February 2022	
		6. Performing Organization Code: N/A	
7. Author(s): Lauren K. Stewart (PI), PhD, PE; Lawrence Kahn (co-PI), PhD, PE; Giovanni Loreto, PhD Patrick Hennigan		8. Performing Organization Report No.: 18-07	
9. Performing Organization Name and Address: Georgia Tech Research Corporation 926 Dalney Street NW Atlanta, GA 30332-0420 Phone: (404) 385-1919 Email: lauren.stewart@ce.gatech.edu		10. Work Unit No.: N/A	
		11. Contract or Grant No.: PI# 0016327	
12. Sponsoring Agency Name and Address: Georgia Department of Transportation (SPR) Office of Performance-based Management and Research 600 West Peachtree St. NW Atlanta, GA 30308		13. Type of Report and Period Covered: Final Report (Sept 2018 – Feb 2022)	
		14. Sponsoring Agency Code: N/A	
15. Supplementary Notes: Prepared in cooperation with the US Department of Transportation, Federal Highway Administration.			

16. Abstract:

American Concrete Institute (ACI) Guide to Mass Concrete defines massive (mass) concrete as "any volume of concrete with dimensions large enough to require that measures be taken to cope with the generation of heat from hydration of the cement and attendant volume change to minimize cracking." Specifically, in the case of drilled shafts, Georgia Department of Transportation defines mass concrete to be any shaft with a greater than six-foot diameter. Once a drilled shaft has been classified as mass concrete, additional general GDOT specifications for mass concrete apply. These specifications detail temperature, material selection, thermal control, placing, and curing. Because the current specification lacks details specific to drilled shafts, a multitude of methods can be used, which can reduce the economic efficiency of the structure. Additionally, because the specifications are vague, the contractor and designer often avoid the specification by installing multiple smaller shafts in place of one single larger shaft. This practice of adding multiple smaller shafts often adds additional cost and the possibility for less effective designs. This project developed best practices and specifications for mass concrete drilled shafts to reduce the hesitance for use in practice and promote better overall construction practice. The objectives of the research are to: (1) understand the major deterrents from utilizing mass concrete for drilled shafts in practice, (2) determine and specify the appropriate thermal conditions, monitoring, and other requirements for drilled shafts specific to Georgia, (3) utilize ongoing GDOT research for temperature control to determine best practices for application on drilled shafts, and (4) make recommendations to GDOT for specifications to advance best practices.

17. Keywords: Drilled shafts, thermal, mass concrete		18. Distribution Statement: No Restriction	
19. Security Classification (of this report): Unclassified	20. Security Classification (of this page): Unclassified	21. No. of Pages: 92	22. Price: Free

Form DOT 1700.7 (8-72) Reproduction of completed page authorized.

GDOT Research Project No. 18-07

Final Report

BEST PRACTICES AND SPECIFICATIONS FOR MASSIVE CONCRETE DRILLED SHAFTS

By
Lauren Stewart, PhD, PE
Associate Professor – School of Civil and Environmental Engineering

Lawrence Kahn, PhD, PE
Emeritus Professor – School of Civil and Environmental Engineering

Patrick Hennigan
Graduate Research Assistant

Georgia Institute of Technology

Giovanni Loreto, PhD
Assistant Professor – Department of Architecture

Kennesaw State University

Georgia Tech Research Corporation

Contract with
Georgia Department of Transportation

In cooperation with
US Department of Transportation
Federal Highway Administration

February 2022

SI* (MODERN METRIC) CONVERSION FACTORS

APPROXIMATE CONVERSIONS TO SI UNITS

Symbol	When You Know	Multiply By	To Find	Symbol
		LENGTH		
in	inches	25.4	millimeters	mm
ft	feet	0.305	meters	m
yd	yards	0.914	meters	m
mi	miles	1.61	kilometers	km
		AREA		
in^2	square inches	645.2	square millimeters	mm^2
ft^2	square feet	0.093	square meters	m^2
yd^2	square yard	0.836	square meters	m^2
ac	acres	0.405	hectares	ha
mi^2	square miles	2.59	square kilometers	km^2
		VOLUME		
fl oz	fluid ounces	29.57	milliliters	mL
gal	gallons	3.785	liters	L
ft^3	cubic feet	0.028	cubic meters	m^3
yd^3	cubic yards	0.765	cubic meters	m^3
		NOTE: volumes greater than 1000 L shall be shown in m^3		
		MASS		
oz	ounces	28.35	grams	g
lb	pounds	0.454	kilograms	kg
T	short tons (2000 lb)	0.907	megagrams (or "metric ton")	Mg (or "t")
		TEMPERATURE (exact degrees)		
°F	Fahrenheit	5 (F-32)/9 or (F-32)/1.8	Celsius	°C
		ILLUMINATION		
fc	foot-candles	10.76	lux	lx
fl	foot-Lamberts	3.426	$candela/m^2$	cd/m^2
		FORCE and PRESSURE or STRESS		
lbf	poundforce	4.45	newtons	N
lbf/in^2	poundforce per square inch	6.89	kilopascals	kPa

APPROXIMATE CONVERSIONS FROM SI UNITS

Symbol	When You Know	Multiply By	To Find	Symbol
		LENGTH		
mm	millimeters	0.039	inches	in
m	meters	3.28	feet	ft
m	meters	1.09	yards	yd
km	kilometers	0.621	miles	mi
		AREA		
mm^2	square millimeters	0.0016	square inches	in^2
m^2	square meters	10.764	square feet	ft^2
m^2	square meters	1.195	square yards	yd^2
ha	hectares	2.47	acres	ac
km^2	square kilometers	0.386	square miles	mi^2
		VOLUME		
mL	milliliters	0.034	fluid ounces	fl oz
L	liters	0.264	gallons	gal
m^3	cubic meters	35.314	cubic feet	ft^3
m^3	cubic meters	1.307	cubic yards	yd^3
		MASS		
g	grams	0.035	ounces	oz
kg	kilograms	2.202	pounds	lb
Mg (or "t")	megagrams (or "metric ton")	1.103	short tons (2000 lb)	T
		TEMPERATURE (exact degrees)		
°C	Celsius	1.8C+32	Fahrenheit	°F
		ILLUMINATION		
lx	lux	0.0929	foot-candles	fc
cd/m^2	$candela/m^2$	0.2919	foot-Lamberts	fl
		FORCE and PRESSURE or STRESS		
N	newtons	0.225	poundforce	lbf
kPa	kilopascals	0.145	poundforce per square inch	lbf/in^2

* SI is the symbol for the International System of Units. Appropriate rounding should comply with Section 4 of ASTM E380. (Revised March 2003)

TABLE OF CONTENTS

LIST OF FIGURES

LIST OF TABLES

EXECUTIVE SUMMARY

Mass concrete is defined by the American Concrete Institute (ACI) as “any volume of concrete with dimensions large enough to require that measures be taken to cope with the generation of heat from the hydration of cement and the attendant volume change to minimize cracking.” Aside from the qualitative description, there is currently no nationally standardized definition of mass concrete in terms of specific volumes and mix designs. Without a clear definition, state Departments of Transportation (DOTs) vary in their definitions and specifications for mass concrete elements.

Georgia Department of Transportation (GDOT) considers mass concrete as any concrete element with any planar dimension of greater than five feet, or greater than six feet in drilled concrete shafts. Because of this definition, mass concrete shafts greater than six feet are often avoided by contractors to avert the monitoring aspect and associated higher costs. This avoidance causes additional work for the DOT because they must review changes to the initial design. Because of this additional work, it is important that the specification diameter (i.e., six feet) is truly the dimension at which mass concrete considerations should be made.

To determine the situations that create mass concrete conditions, an experimental and computational effort was completed. Through field monitoring and laboratory experiments, this research explored the effects of boundary condition (air, soil, water) and mix design on the concrete. The research concluded that the boundary conditions of a drilled shaft affect its maximum temperature as well as the temperature gradient at the

edge of the shaft. Therefore, it is recommended that these conditions be considered in current mass concrete specifications. In shafts that are bounded by water, it is recommended to monitor the temperature gradients closer to the edge of the shaft instead of the currently used linear approximation from the core to the edge region, which does not account for significantly higher local maximum gradients.

CHAPTER 1. INTRODUCTION

MOTIVATION

The high temperatures generated by concrete with large dimensions have been long known to have potentially damaging effects on structures. If not accounted for, structures containing mass concrete elements can experience high thermal stresses, which can cause thermal cracking. This cracking results in a loss of structural integrity and monolithic action.[1] Several methods have been developed to help reduce the maximum temperature and the temperature differentials in these massive concrete elements. The three main methods of heat mitigation are precooling the aggregates used in the concrete mix to lower the initial concrete temperature, altering the mix design of the concrete to have a lower heat of hydration, and installing a post-cooling system to actively remove heat as the cement hydrates .[2]

Although the effects of unmitigated mass concrete are well known, there has been little consensus on what should be considered mass concrete. The American Concrete Institute (ACI) maintains a general definition with specific temperature limits, whereas several states' Departments of Transportation (DOT) have made specific definitions and specifications concerning mass concrete.[3] State DOTs range from having no specifications, to defining mass concrete as elements with dimensions of three feet or greater. The Georgia Department of Transportation (GDOT) considers mass concrete as any concrete element with a dimension greater than five feet, or greater than six feet in drilled concrete shafts.[4]

Through experimental and computational investigations, this research explores the conditions that effect the temperatures in the concrete and develops methods to accurately monitor and limit temperatures in a drilled shaft to prevent the manifestation of negative effects from mass concrete.

RESEARCH OBJECTIVES

The objectives of this research are as follows:

1. To understand the implementation resistance and performance issues with mass concrete drilled shafts through observation and the instrumentation of construction sites of GDOT or neighboring states bridges and expert interviews.

2. To quantify the thermal conditions of drilled shafts of various diameters and conditions that are specific to Georgia.

3. To utilize ongoing thermal research and other states' best practices for application on drilled shafts.

4. To demonstrate best practices in the laboratory through validation experiments.

5. To draft recommended practices for GDOT drilled shaft specifications thus promoting use in practice while increasing performance reliability.

REPORT ORGANIZATION

Chapter 2 of this report gives a literature review with current mass concrete practices. Specifically, it summarizes the specifications used by other state DOTs. Chapter 3 describes the site visits that were conducted throughout the project and discusses the monitoring effort. Chapter 4 details the laboratory effort and provides results that study

the effects of boundary conditions on performance. Chapter 5 contains details on the computational model validation process as well as parametric studies on shaft diameter and boundary condition. Finally, Chapter 6 provides the conclusions and recommendations.

The seven appendices contain the mix designs for field and Sonotube shafts (Appendix A), bridge drawings (Appendix B), field monitoring results (Appendix C), laboratory test results (Appendix D), and computational modeling procedure (Appendix E).

CHAPTER 2. LITERATURE REVIEW

This chapter reviews the existing definitions, research, and construction practices involving mass concrete and its applications. This covers mass concrete specifications that vary by state as well as GDOT standards and practices. Finally, field monitoring practices, experimental techniques and modeling strategies are included.

MASS CONCRETE

Definition

In ACI CT-21, ACI identifies mass concrete with the following definition:

> *. . . any volume of structure concrete in which a combination of dimensions of the member being cast, the boundary conditions, the characteristics of the concrete mixture, and the ambient conditions can lead to undesirable thermal stresses, cracking, deleterious chemical reactions, or reduction in the long-term strength as a result of elevated concrete temperature due to heat from hydration.*

Materials

The materials used in mass concrete are generally the same as concrete used in standard applications. The mix designs can be varied to alter the temperature profile of the concrete using various cementitious materials and admixtures.[2]

Issues

If not accounted for, structures containing mass concrete elements can experience high thermal stresses which can cause thermal cracking. This cracking results in a loss of structural integrity and monolithic action.[1] Due to the large nature of mass concrete

elements, it could be costly and time consuming to replace an element that is not acceptable due to crack formation.

TEMPERATURE MITIGATION METHODS

Precooling

A process known as precooling is used to help reduce the peak temperature rise of the concrete during curing. The lower initial temperature will reduce the final maximum heat achieved from the cement hydration. This method involves cooling the aggregates and water prior to mixing the concrete batch; thus, pouring the concrete will occur at the lowest possible initial temperature. This can be accomplished in many ways such as batching concrete during the night when it is cooler, placing concrete during cooler seasons, refrigerating the batch water, or even replacing some of the batch water with ice.[2]

Mix Design

The concrete mix can include certain admixtures to reduce the heat of hydration during the curing process. Because heat generated during curing comes from the cement being hydrated, if the total amount of cement is reduced, it reduces the heat generated. The use of slag or fly ash in place of cement can greatly reduce the heat of hydration, which will reduce the peak temperature and thermal gradients.[1]

Post-cooling

Another method of reducing the maximum temperature during curing is to install a post-cooling system. This usually consists of embedded pipes that circulate refrigerant to remove heat. Water or a mixture of water and either antifreeze or brine is often used to

reduce the freezing point of the refrigerant water. Air has also been used previously in desert climates where water is scarce.[2]

Surface Insulation

To prevent a rapid cooling of the mass concrete element's surface, it is recommended to place surface insulation around exposed mass concrete during the early stages of curing. If the exterior surface of the concrete cools much faster than the core, it can cause a high thermal strain near the surface, which would result in crack formation known as thermal shock.[2]

MASS CONCRETE SHAFT SPECIFICATIONS

Shaft Designs and Rules

State agency specifications vary greatly in their definition of mass concrete and its temperature limits. Some states consider concrete elements with a least dimension greater than three feet as mass concrete, whereas other states do not have any definition.[5]

Table 1 illustrates the vast differences in state mass concrete definitions. States omitted from Table 1 lack any provisions for mass concrete.

GDOT Procedures

GDOT definitions and procedures for mass concrete can be found in GDOT Special Provisions (SSP) 500. GDOT SSP 500 uses the same general definition for mass concrete as the ACI but has specific geometric limits that require design considerations. These include any concrete element, excluding drilled shafts, with a least dimension greater than five feet. Any element with construction joints less than five feet that have a

volume-to-surface area ratio greater than or equal to one foot is also considered mass concrete.[4] GDOT considers drilled shafts exceeding six feet as massive concrete.[5]

Table 1. Comparison of state DOTs' specifications for mass concrete.

State DOT	Least dimension for general concrete sections	Least dimension (diameter) explicitly for drilled shaft	Reference
(a) Same dimension limits for all concrete members including drilled shafts			
Idaho	4 ft		Section 502.03.F.4, (ITD, 2018)
Illinois	5 ft		Section 1020.15, (IDOT, 2015)
Iowa	5 ft (footings), 4 ft (members other than footings)		Section 090042.01, (Iowa DOT, 2010)
Louisiana	4 ft		Section 901.12.1, (La DOTD, 2016)
Rhode Island	3 ft		Section 607.01.1, (RIDOT, 2016)
Virginia	5 ft		Section I, (VDOT, 2016)
(b) Different dimension limits for drilled shafts and other concrete members			
Florida	3 ft	6 ft	Section 1.4.4.C, (FDOT, 2018)
Georgia	5 ft	6 ft	Section 500.3.05.AM, (GDOT, 2013)
Ohio	5 ft	7 ft	Section 511.04.A, (ODOT, 2016)
(c) Dimension limits explicitly for drilled shafts			
California	-	8 ft	Section 49-3.01B, (Caltrans, 2018)
Texas	-	5 ft	Section 416.3.6, (TxDOT, 2014)
(d) Dimension limits only apply to concrete members other than drilled shafts			
Kentucky	6 ft	Not considered as mass concrete	Section 1.0, (KYTC, 2012)
Minnesota	4 ft	Not considered as mass concrete	Section DBSB-2401.27, (MnDOT, 2007)
South Carolina	5 ft (6 ft for circular sections)	Not considered as mass concrete	Section 702.4.2.5, (SCDOT, 2007)
Washington	6 ft	Not considered as mass concrete	Section 5.1.1.H, (WSDOT, 2018)
West Virginia	4 ft	Not considered as mass concrete	Section 601.1.1, (WVDOT, 2010)

Mass concrete elements are limited by GDOT SSP 500 to a maximum internal temperature of 158 °F. The temperature difference between the core and the exterior surface portion may not exceed 35 °F, with the exterior surface portion temperature measured 2–6 inches from the closest surface, at the depth of reinforcing steel.[4] GDOT SSP 500 requires temperatures to be monitored in a minimum of four locations in each mass concrete element. The monitored locations are at the center of mass of the pour, the mid-point of the side closest to the center of mass, and the midpoint of both the top and bottom surfaces of the pour.[4]

EXAMPLE MASS CONCRETE PROJECTS

Pocahontas Parkway

An example of a bridge project using mass concrete is the Pocahontas Parkway located in Richmond, Virginia, across the James River. The bridge required the placement of eight-foot diameter drilled shafts extending 60–80 feet below ground. To reduce the peak temperature, the contractors opted to use a mix design consisting of 75% slag and 25% Portland Cement Concrete (PCC) to reach the required strength of 4,350 psi. Temperature sensors were placed every six feet in the core of each shaft and recorded a peak temperature of 155 °F, which is less than the VDOT maximum requirement of 170 °F.[6]

Sellwood Bridge

The 1,976-foot Sellwood Bridge, located across the Willamette River in Portland, Oregon used several mass concrete piers. The largest concrete elements were the 22 piers, each with a diameter of 10 feet. To prevent the harmful effects of mass concrete, a post-

cooling system was installed in the drilled shafts that continuously circulated river water.[7]

BNSF Historic Memphis Bridge

The project to replace the BNSF Historic Memphis Bridge over the Mississippi River in Memphis, Tennessee, used 10-foot diameter drilled concrete shafts. The engineers on this project decided to mitigate high temperatures by focusing on reducing the initial concrete placement temperature as well as using a post-cooling system. Aggregate stockpiles were stored under canopies and sprinkled with 34 °F water, 50–75% of the concrete batch water was replaced with ice, and the remaining batch water was 34 °F. The post-cooling system recycled the same water from storage tanks but replaced the water used when it reached a temperature of 80 °F.[8]

STRATEGIES TO CHARACTERIZE MASS CONCRETE

Field Monitoring Methods

Temperature sensors are used to monitor the temperature of concrete components prior to batching. Also, sensors embedded in the concrete are used to monitor temperatures during placement and curing as well as to monitor any post-cooling system. Sensors that are commercially available and accurate to ± 2 °F are adequate for stockpile and concrete curing monitoring.[2]

Experimental Techniques

Experimental methods typically involve full scale laboratory tests. The lab tests monitor the temperature, and sometimes the strain, of a concrete specimen during curing. Key data points often include the maximum temperature as well as the temperature differential

between the core of the sample and the closest surface. In 2018, Singh and Rai performed an experiment that characterized mass concrete in the laboratory environment by constructing a series of 600-millimeter (2.0-feet) concrete cubes and collecting temperature data at eight points of interest.[9] In 2015, Yikici characterized mass concrete in a laboratory setting in a similar fashion by constructing six-foot cubes and collecting temperature data.[10]

CHAPTER 3. FIELD MONITORING

To characterize the temperature response of mass concrete in situ, a field monitoring effort was conducted on a single drilled shaft that met the current GDOT mass concrete specification. This chapter describes the collection of temperature and strain data from an active bridge construction project near Macon, Georgia. The project that was under construction was the Martin Luther King Junior Boulevard bridge over the Ocmulgee River, located in Bibb County, GA as seen in Figure 1.

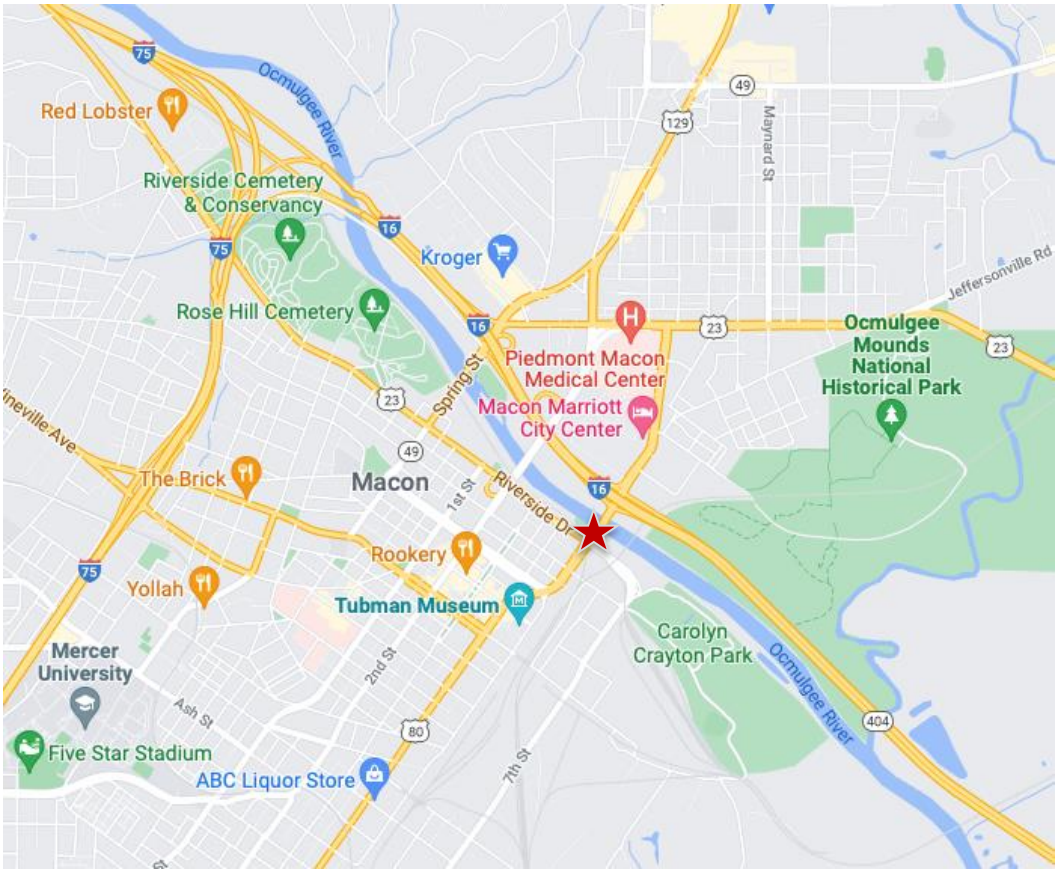

Figure 1. Map. Location of the field monitoring

The Martin Luther King Junior Boulevard bridge project was selected for field monitoring because it contained drilled shafts designated as a mass concrete under GDOT

SSP 500. The casting of one of the shafts was also conveniently scheduled during the research phase of this project and in proximity to Georgia Institute of Technology. Figure 2 shows the typical details of the shafts that were designed for the project. The shaft that was monitored had a cross section shown in Figure 2 and reached a depth of 55.5 feet below the surface. Additionally, it was bounded fully in soil because it was located approximately 20 feet from the bank of the Ocmulgee River, as shown in Figure 3Figure 3.

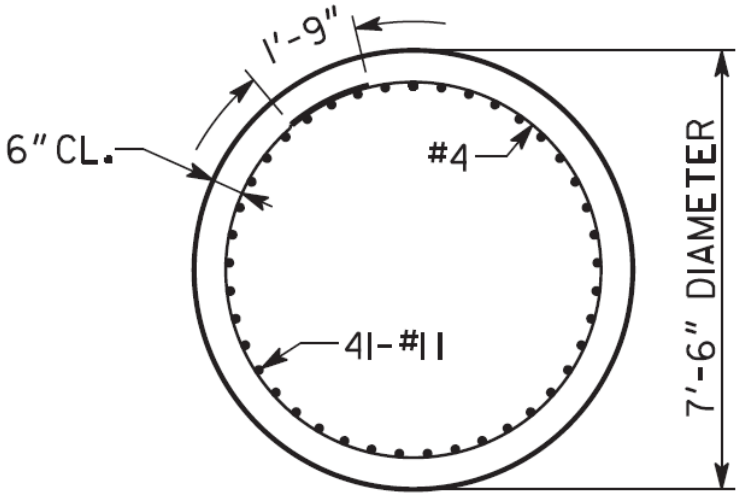

Figure 2. Engineering drawing. Typical drilled shaft cross section of the GDOT projected that was monitored

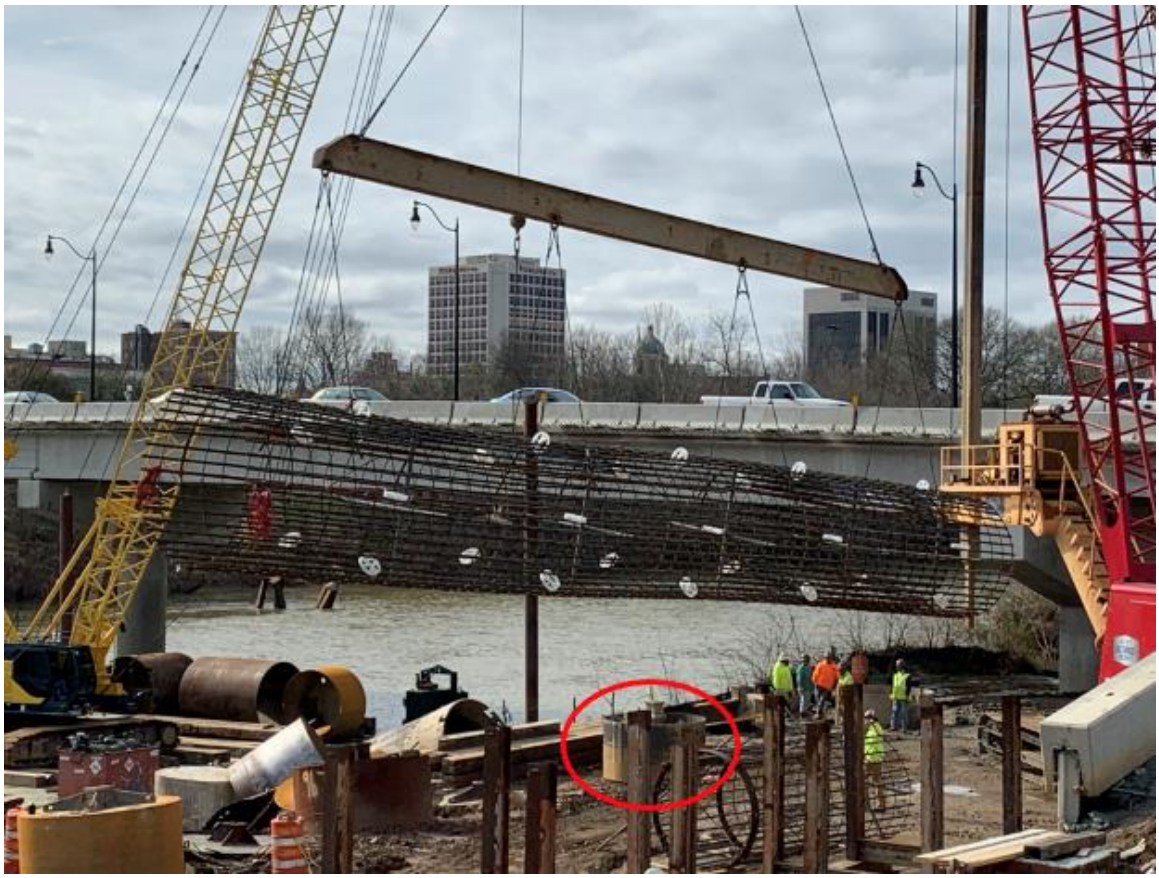

Figure 3. Photo. Location of drilled shaft near the bank of the Ocmulgee River

The bridge project employed two methods to mitigate the heat generated during curing. The first method employed a mix design that met GDOT Class AA, caisson specifications while using 70% slag and 30% cement. The mix design for the pour is given in Appendix A. Also, the designers elected to use a post-cooling system consisting of a loop with five longitudinal runs of steel pipe using Ocmulgee River water as refrigerant, given in Appendix B.

INSTRUMENTATION

Nineteen Geokon model 3800 thermistors were used to collect temperature data and five Geokon model 4200L low modulus vibrating wire strain gauges were used to collect strain data. Each sensor was connected to one of two Geokon LC-2x16 data acquisition

systems that collected data on a 30-minute interval for 10 days. The thermistors were placed in a line across the diameter with three-inch spacing for the first and last five sensors and six-inch spacing for the nine interior sensors, as shown in Figure 4. The vibrating wire strain gauges were spaced evenly across the diameter.

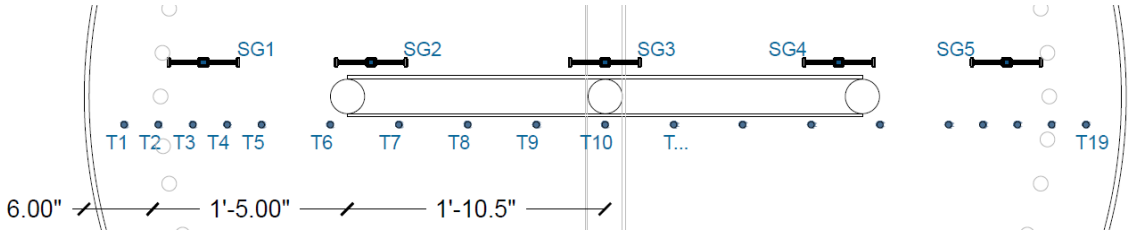

Figure 4. Schematic. Sensor layout across the diameter of the shaft at a depth of 25 feet below finished elevation. The items labeled "SG#" are sensor names for strain gauges, whereas the items labeled "T#" are thermistors

The sensors were embedded along the same line across the diameter at a depth of 25 feet below the surface elevation. Sensors were attached to three lengths of fiber-reinforced polymer (FRP) bar that was fixed to the rebar cage on either side as well as the cooling pipes. Three lengths of FRP bar were used to facilitate the lowering of the post-cooling system after the rebar cage was in place. Figure 5 shows one side of the sensors and FRP bar attached to the rebar cage. Figure 6 shows the sensors and FRP bar attached to the cooling pipes. The shaft with the sensor cables protruding from the finished surface after three days of data collection can be seen in Figure 7.

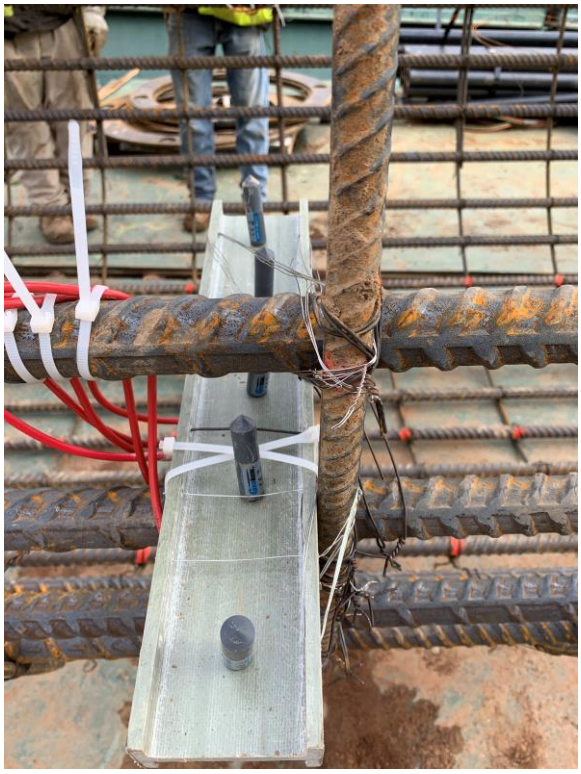

Figure 5. Photo. Sensors attached to one side of the rebar cage.

Figure 6. Photo. Sensors and FRP bar attached to the post-cooling system

Figure 7. Photo. Cables protruding from shaft three days after placement

GEORGIA TECH MONITORING RESULTS

Detailed results from the monitoring are given in Appendix C. The shaft reached a peak core temperature of 127 °F. The maximum differential between the core temperature and three inches from the surface was 25 °F. The maximum differential between the core and the exterior surface portion, defined by GDOT SSP 500 as the depth of rebar up to six inches from the surface, was 20 °F. Figure 8 gives a plot of the core temperature of the shaft with respect to time after concrete placement from thermistor T10. Figure 9 is a plot of the temperature differential from the core and one side of the shaft at a depth of three and six inches. Figure 10 is a plot of temperature from sensor T9, which was affixed directly adjacent to the post-cooling system. The figure shows three distinct drops in temperature when the contractors initiated the post-cooling system. The contractors

initiated the post-cooling system only when their internal temperature sensors approached 130 °F.

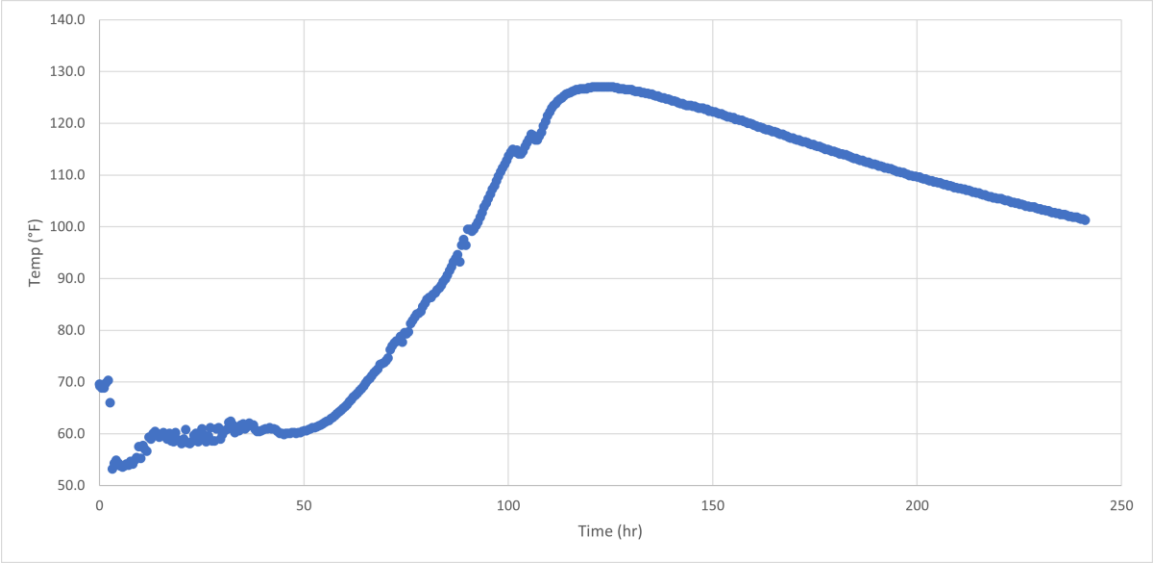

Figure 8. Graph. Shaft's core temperature

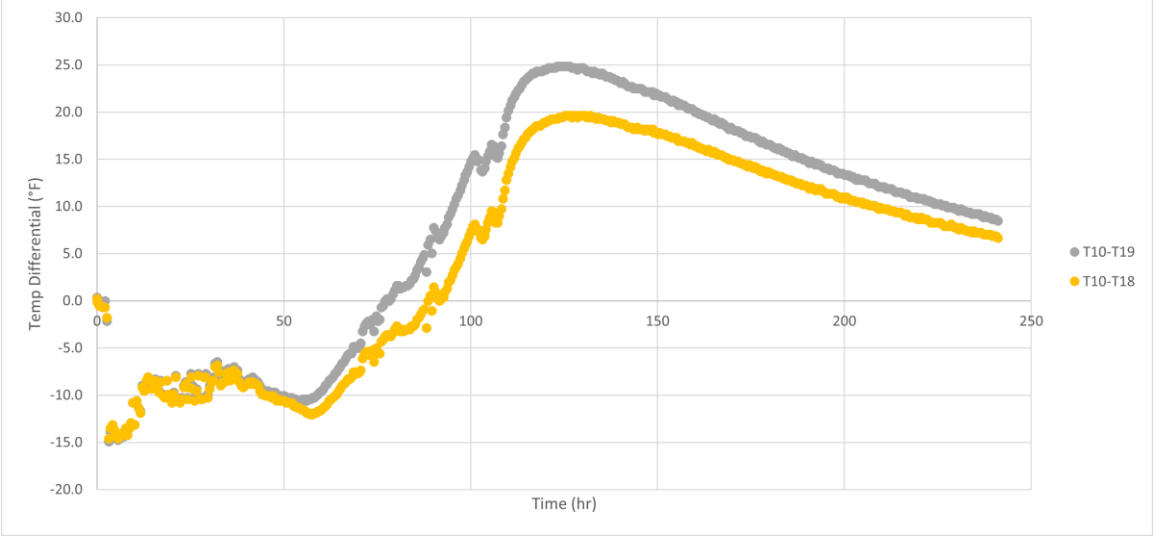

Figure 9. Graph. Temperature differential from the core to 3 inches (T10-T19) and 6 inches (T10-T18) from the surface

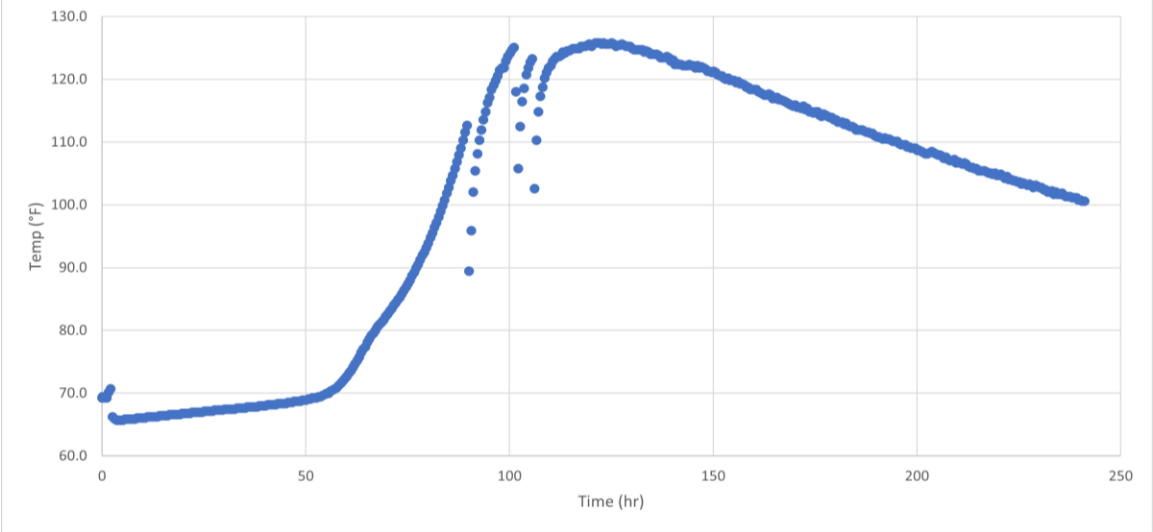

Figure 10. Graph. Concrete temperature immediately adjacent to a post-cooling pipe

CHAPTER 4. LABORATORY EXPERIMENTS – SONOTUBE CASING

This chapter describes the experimental testing that was conducted in the Structural Engineering and Materials Laboratory at Georgia Institute of Technology. To understand the effects of boundary condition on the concrete, both temperature and strain data were collected on three mock drilled shaft specimens with the three distinct boundary conditions of soil, water, and air with Sonotube casing. Two additional experiments of shafts with steel casings were conducted in water.

TEST SPECIMEN

Five specimens were constructed during the testing phase of this research. Each specimen had the same mix design that was used in the field monitoring project, which was Class AA, caisson specified with 70% slag and 30% type I cement. The five specimens were four-foot diameter, three-foot-tall cylinders with the rebar configuration shown in Figure 11. Each specimen had one of three boundary conditions: air, water, and soil.

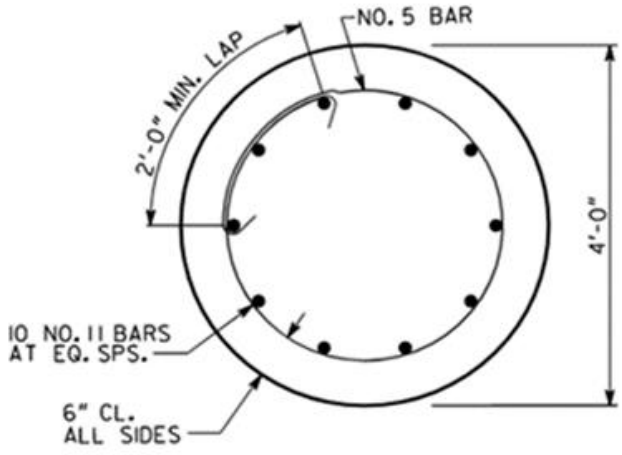

Figure 11. Engineering drawings. Dimensions and rebar layout of each specimen tested in the lab

INSTRUMENTATION

The same Geokon instrumentation described in the field monitoring section was also used for the laboratory tests. There were 15 thermistors spaced along the diameter at the mid-height of the specimen in the configuration shown in Figure 12. There was a total of five strain gauges with a diametrically oriented strain gauge located on each side of the rebar cage along the same line as the thermistors. In the center of mass of each specimen were three more strain gauges. The configuration of the center strain gauges for the air sample can be seen in Figure 13. The configuration of the three center strain gauges was modified for the water and soil samples to be that of a Rosette configuration, which can be seen in Figure 14. Like the field monitoring mounting, each sensor was affixed to a FRP bar, as seen in Figure 15. The data loggers also recorded temperatures inside of the data logger box. These temperatures were used as the ambient air temperatures during data collection.

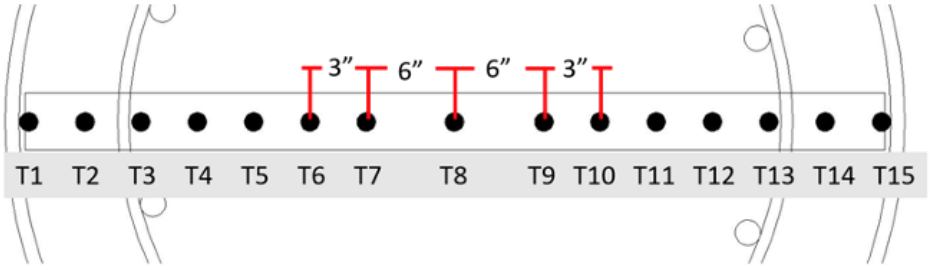

Figure 12. Schematic. Thermistor layout at mid-height of the lab specimens. The black dots represent thermistor locations with sensor names labeled "T#"

Figure 13. Photo. Vibrating wire strain gauge sensor configuration at the center of the air specimen

Figure 14. Photo. Strain rosette configuration used in the center of the water and soil specimens

Figure 15. Photo. Sensor configuration used in both the water and soil samples

TEST MATRIX

The test matrix for the five experiments is given in Table 2Table 2. The first two letters in the test name represent the casing type: “C” for cardboard Sonotube and “S” for steel. The second letter represents the boundary: “A” for air, “S” for soil, and “A” for air. The final letter gives the concrete mix: “A” for mix A, which was used in the field experiments and “B” for a similar mix with higher w/c ratio (see Appendix A).

Table 2. Laboratory experiments test matrix

Experiment Name	Casing	Boundary	Mix
Test C-A-A	Cardboard	Air	A
Test C-S-A	Cardboard	Soil	A
Test C-W-A	Cardboard	Water	A
Test S-W-B	Steel	Water	B
Test S-W-A	Steel	Water	A

TEST C-A-A: CARDBOARD CASING WITH AIR BOUNDARY, MIX A

Setup

The air boundary condition test was the first test conducted in the laboratory. Cylindrical cardboard formwork with an outside diameter of four feet was used for all specimens. The rebar was assembled in the configuration shown in Figure 11, with six-inch spacing between the rebar hoops. To begin, a layer of two-inch-thick polystyrene insulation was placed on the concrete floor of the laboratory with dimensions large enough to cover the cross-sectional area of the formwork. Then, a layer of 0.75-inch plywood of the same area was set on top of the insulation. The formwork was then fixed to the plywood using duct tape on the bottom of the exterior. Silicone caulking was then applied to the inside surface where the formwork joined the plywood to prevent spillage during casting. Figure 16 shows a plan view of the assembled experimental setup.

Figure 16. Photo. Plan view of the completed experimental setup prior to attaching the pickup points. Not pictured is the layer of polystyrene underneath the plywood

After the above steps were completed, the rebar cage of the dimensions specified previously was assembled by twisting steel wire around the points of intersection between the longitudinal rebar and hoops. The sensors used in the project were then attached to an FRP wide flange beam. The wires for the thermistors were fed through holes drilled at the desired temperature locations in the web of the FRP beam. The wires for the two thermistors nearest to the formwork were fed from the interior of the formwork to the exterior at the desired location through drilled holes. The five strain gauges were then attached to the FRP beam. Once all the sensors were attached to the FRP beam, the beam was then attached to the rebar cage at the mid-height of the specimen by twisting steel wire. The cage and sensors were then lowered by crane into the formwork.

Once the cage and sensors were lowered into the formwork, six-inch pieces of 2x4s were placed along the circumference of the uppermost rebar hoop to obtain an even concrete cover along the circumference, which also provided much needed rigidity to the rebar cage. Two 10-foot number eight rebar lengths were then bent by 180 degrees about their midpoint and tied to the rebar cage using steel wires to provide a pickup point to move the specimen in the future. A simple 2x4 frame was constructed around the pickup points to secure the formwork to the layer of plywood during concrete placement. This was done by attaching two vertical 2x4s to a horizontal 2x4 that was flush across the top of the formwork. The vertical 2x4s were then affixed to the plywood. Two of these simple frames were placed around each specimen. Figure 16 shows a completed experimental setup prior to the concrete placement. Not pictured is the layer of polystyrene insulation under the plywood layer nor the rebar pickup points attached to the reinforcement.

During concrete placement, a sheet of plywood was held at an angle over the strain gauges to prevent the flowing concrete from misaligning the precariously attached sensors as shown in Figure 17. Special care was also taken to avoid affecting the FRP bar while consolidating the concrete using a vibratory compactor. Upon completion of casting operations, the surface of the concrete was smoothed using trowels, and another layer of two-inch polystyrene insulation was placed on top of the concrete.

Figure 17. Photo. Plywood shield used to protect sensors during concrete placement

Concrete placement occurred on July 16, 2021. The concrete was specified to be delivered with an eight-inch slump but was found to be less than ½ inch upon delivery. To increase workability, an unspecified amount of water was then introduced to the mix on site to increase the slump to nine inches. Figure 18 shows the air specimen after concrete and polystyrene placement.

Figure 18. Photo. Test C-A-A specimen after concrete and polystyrene placement

Results

The temperature data from the individual gauges is included in Appendix D. Cracking was apparent in the specimen, as shown in Figure 19. The maximum crack size in the specimen was 0.03 inches, with an average crack size of 0.02 inches. The cracks formed in the specimens bounded by air and water appeared to follow a circumferential pattern approximately three to six inches from the surface at the location of the steel reinforcement.

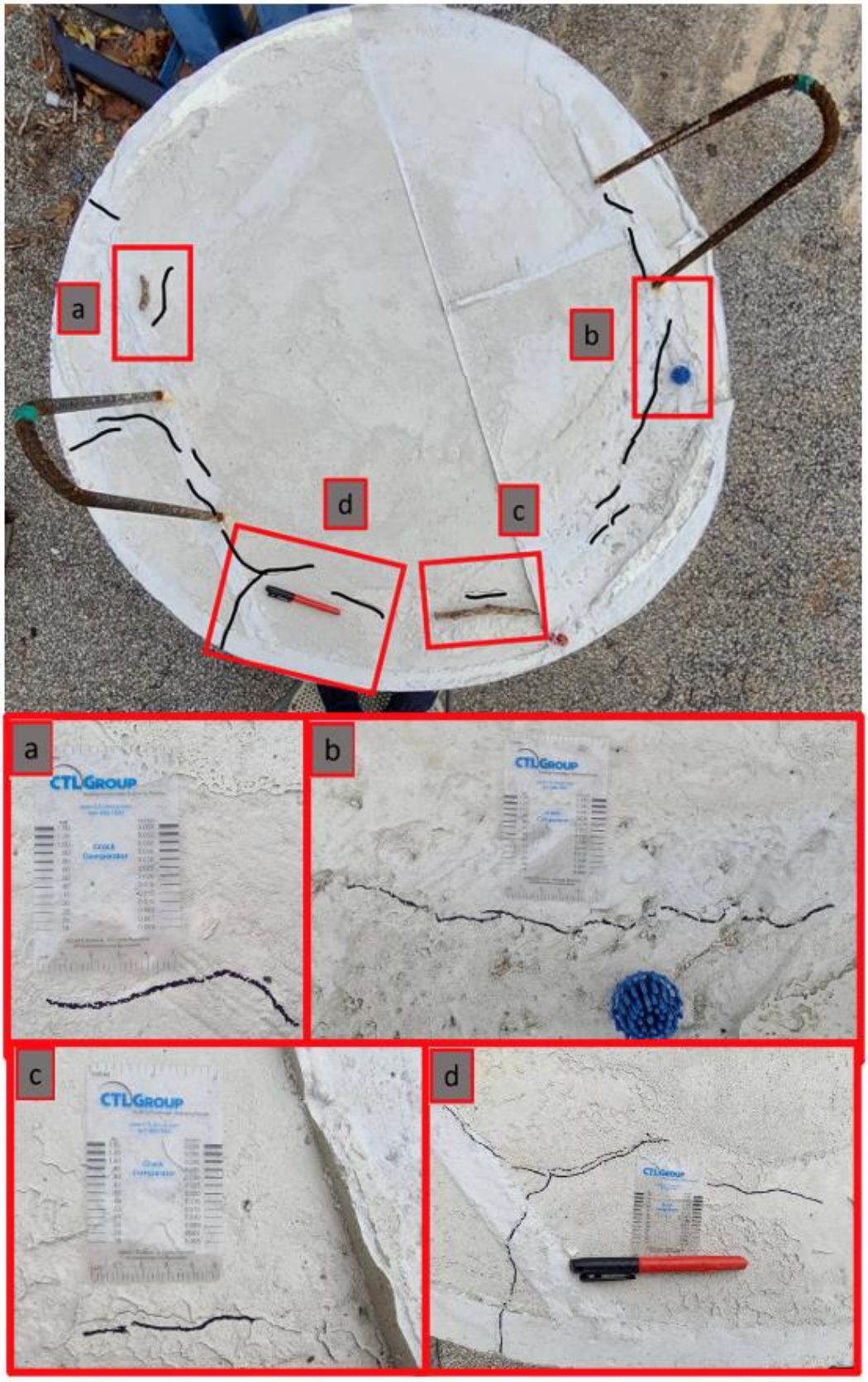

Figure 19. Photo. Cracking observed in Test C-A-A

TEST C-S-A: CARDBOARD CASING WITH AIR BOUNDARY, MIX A

The specimen encased in soil had very few, although significant, differences in the setup from Test C-A-A. Primarily, an 1,100-gallon water storage tank was obtained to facilitate the soil encasement. Figure 20 shows the drawings for the tanks used in this research. The tank was not acquired due to its water capacity but rather was selected due to its diameter being 87 inches with a sidewall height of 40 inches. This would allow for the 48-inch diameter concrete specimen to be placed concentrically inside the tank with an 18-inch soil layer completely encasing the circumference. This provided an easy, clean, expedient, and cost-effective way to conduct the test in a laboratory setting. The tank had to be modified by using a hand saw to remove the ceiling of the tank, allowing the setup to be constructed inside.

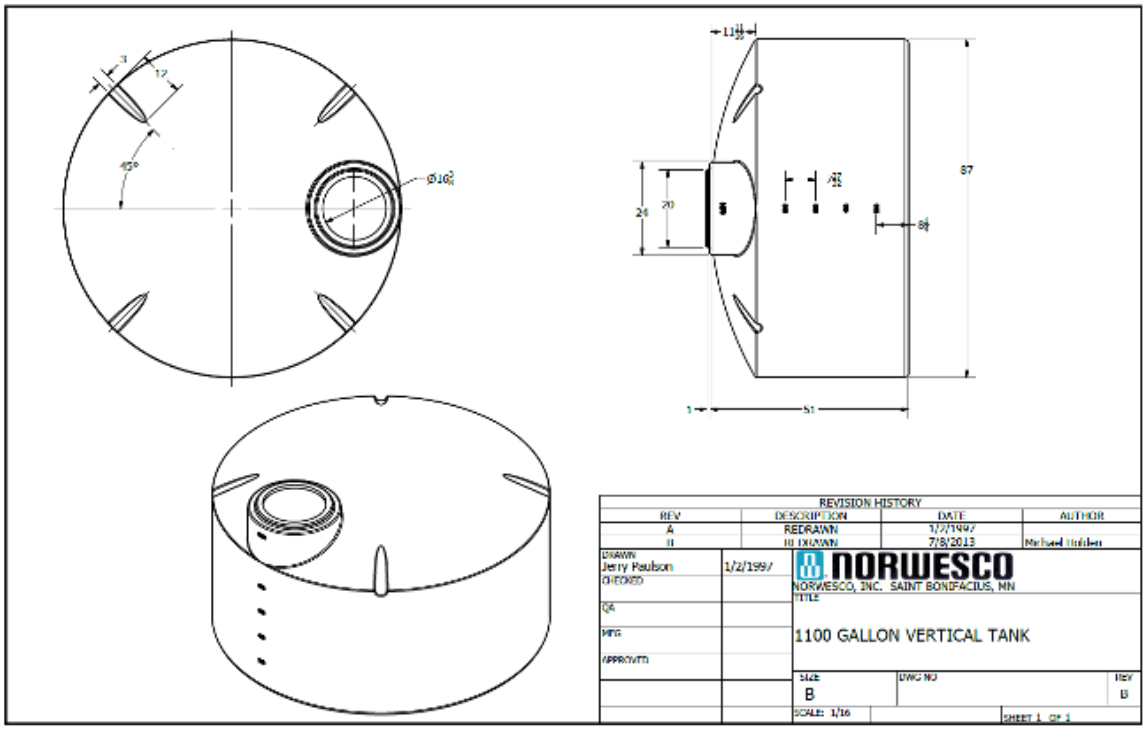

Figure 20. Engineering drawings. Dimensions for the tanks used (courtesy of NORWESCO)

A four-inch layer of polystyrene insulation large enough to cover the cross section of the tank was placed on the laboratory floor. Then the tank was placed on top of the insulation. A layer of plywood was placed on the bottom of the inside of the tank with the rest of the setup being identical to the air test. The only difference was that the thermistors closest to the surface were affixed to small protrusions of FRP bar against the interior surface of the formwork instead of through drilled holes in the formwork. Also, the orientation of the central strain gauges was slightly altered as discussed previously. Finally, an additional thermistor was buried in the soil at the mid-height of the tank, about six inches from the formwork along the same diametric line as the FRP bar.

After the specimen setup was constructed inside the tank to include the formwork, rebar cage, sensors, and pickup points, spare topsoil provided by the groundskeeper team at Georgia Institute of Technology was placed outside the formwork in the tank. Because it was excess topsoil, it contained large amounts of detritus, mostly organic matter. The topsoil was continuously compacted using a steel hand tamper. Figure 21 shows a completed setup prior to concrete placement for the specimen bounded in soil. Concrete placement for the soil sample was conducted on August 23, 2021, in a similar manner to the placement of the air specimen. The slump was found to be satisfactory upon delivery and no additional water was added to the mix. Finally, after the conclusion of the placement, a two-inch layer of polystyrene insulation was placed on the surface of the concrete. Figure 22 shows the soil specimen after concrete placement.

Figure 21. Photo. Test C-S-A specimen prior to concrete placement

Figure 22. Photo. Test C-S-A specimen after soil placement

Results

The temperature data from the individual gauges is included in Appendix D. Almost no cracking was apparent in the Test C-S-A specimen, as shown in Figure 23. The few cracks in the Test C-S-A specimen had a maximum crack size of 0.01 inches, with an average of 0.005 inches

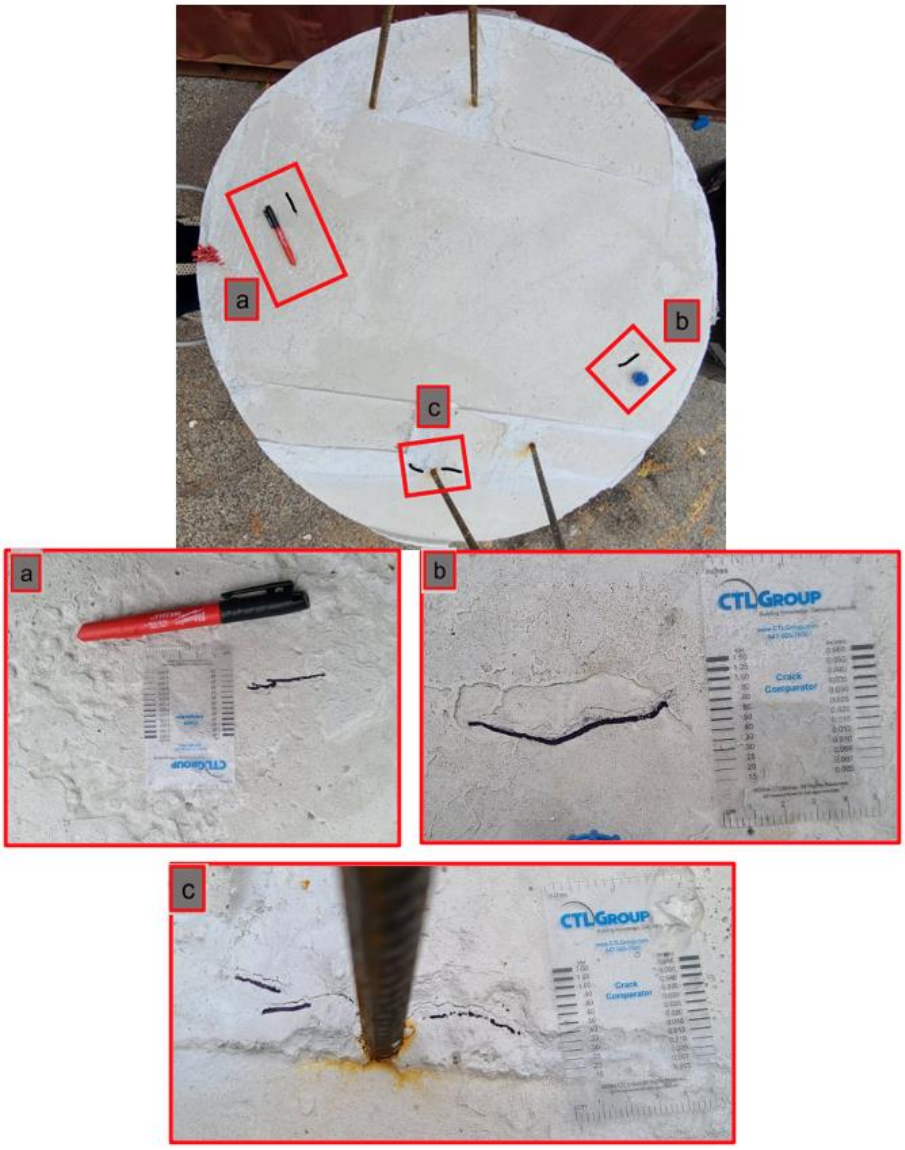

Figure 23. Photos. Cracking observed in Test C-S-A

TEST C-S-A: CARDBOARD CASING WITH WATER BOUNDARY, MIX A

The water specimen had a few significant differences from the soil specimen. The setup was identical to the soil setup, except the cardboard formwork was wrapped in a layer of thick plastic wrap to increase its water resistance. The exact same tank was procured for this test as used in soil test. Also, a fitting for a hose bib was installed on the drain at the bottom of the tank to control the effluent flow rate. This would facilitate the controlled drainage of the effluent from the test. The remainder of the formwork, plywood, rebar cage, and pickup points were identical to those used in the soil test. An additional thermistor was also placed in the water. Figure 24 shows the completed water specimen setup prior to concrete placement.

Figure 24. Photo. Water specimen experimental setup prior to concrete placement

Concrete placement was concurrent with the soil specimen and was placed using the same batch in the same delivery truck. Immediately after placement, a water hose was clamped to the top of the tank on the opposite side of the tank from the drain. The tank was quickly filled with water at maximum inflow. Once the tank was full, the influent and effluent were calibrated to be as close to equal flow as possible with the effluent being slightly greater. This would prevent any overflows in the lab outside of business hours. Also, a water sensor alarm was placed at the top of the tank to emit noise and alert anyone nearby when the water approached the top of the tank. Figure 25 shows the water sample after casting and the tank filled with water.

Figure 25. Photo. Test C-W-A specimen after casting and filling the tank with water

Maintaining a constant water level was challenging. A constant, steady water level extremely near to the top of the tank with an influent and effluent high enough to maintain a constant water temperature would have been the ideal situation. However, the effluent was not fast enough to provide a refresh rate to maintain a constant temperature.

It was also very difficult to maintain the water level near the top of the tank, and it would frequently drop by one to two feet overnight. In future tests, this system was modified.

Results

The temperature data from the individual gauges is included in Appendix D. Cracking was apparent in the specimen, as shown in Figure 26. The maximum crack size in the specimen was 0.03 inches, with an average crack size of 0.02 inches. There were significantly more cracks than the previous two specimen. The cracks formed in the specimens bounded by air and water appeared to follow a circumferential pattern approximately three to six inches from the surface at the location of the steel reinforcement.

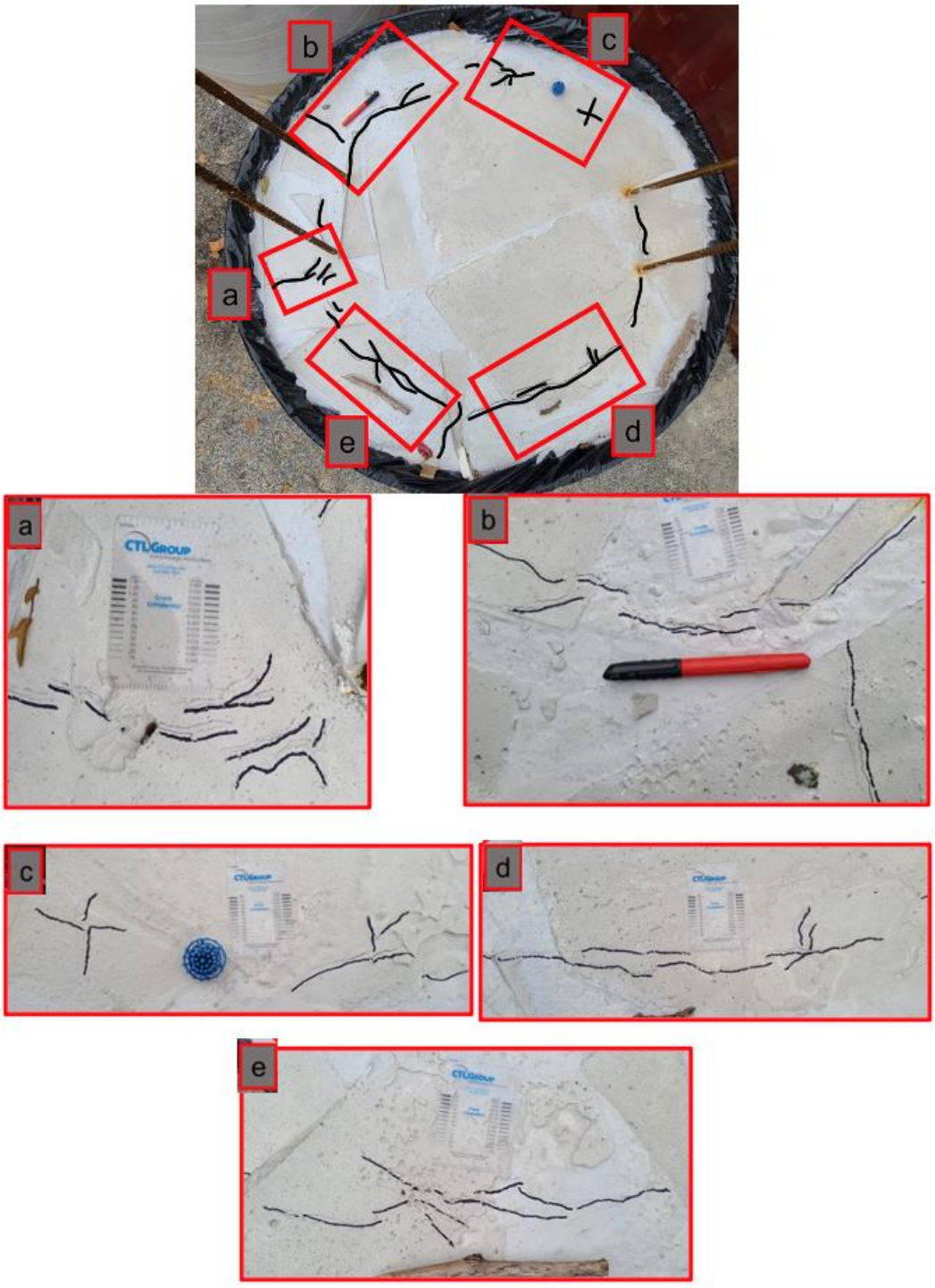

Figure 26. Photos. Cracking observed in Test C-W-A

TEST S-W-B: STEEL CASING WITH WATER BOUNDARY, MIX B

Setup

The steel casing in water specimen had a few significant differences from the specimens discussed previously. The main difference was that a 7/16 in thick steel casing was used instead of a cardboard Sonotube. The exact same tank was used for this test as was used in the previous test. Because maintaining a constant water level was challenging previously, the outflow hose was increased in diameter and an overflow pipe was also installed. Figure 27 shows the completed water specimen setup with the new outflow system, which achieved desired results. The concrete for the specimen had a higher water-to-cementitious material ratio due to an un-workable slump upon delivery.

Figure 27. Photo. Test S-W-B specimen experimental setup

Results

Detailed results for each temperature gauge are given in Appendix D. Cracking was apparent in the specimen, as shown in Figure 28. The cracks were not as prominent as the water (C-W-A) and air (C-A-A) tests previously but was more than the soil test (C-S-A). The maximum crack size in the samples was 0.02 inches, with an average crack size of 0.02 inches. All visible cracks measured the same size. The cracks formed in the specimens again appeared to follow a circumferential pattern approximately six inches from the surface at the location of the steel reinforcement.

TEST S-W-A: STEEL CASING WITH WATER BOUNDARY, MIX A

Setup

This test also featured a steel casing with a water boundary condition. This test was a repeat of the Test S-W-B, except that this mix was identical to the mixes in the first four experiments (Mix A).

Results

Detailed results for each temperature gauge are given in Appendix D. Cracking was apparent in the specimen, as shown in Figure 29. The maximum crack size in the samples was 0.02 inches, with an average crack size of 0.002 inches. There were very few cracks, and they did not follow the circumferential pattern, similar to other tests.

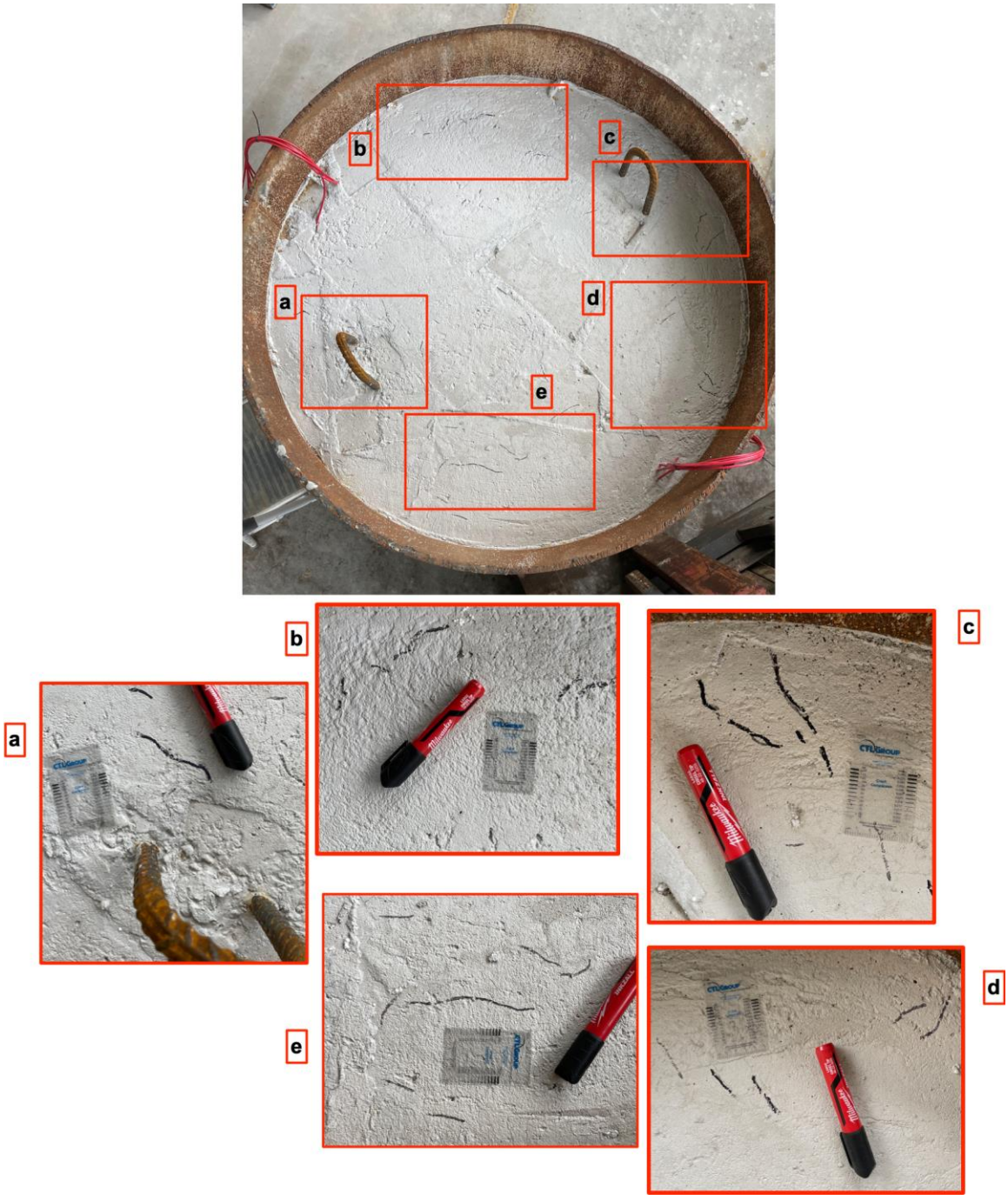

Figure 28. Photos. Cracking observed in Test S-W-B

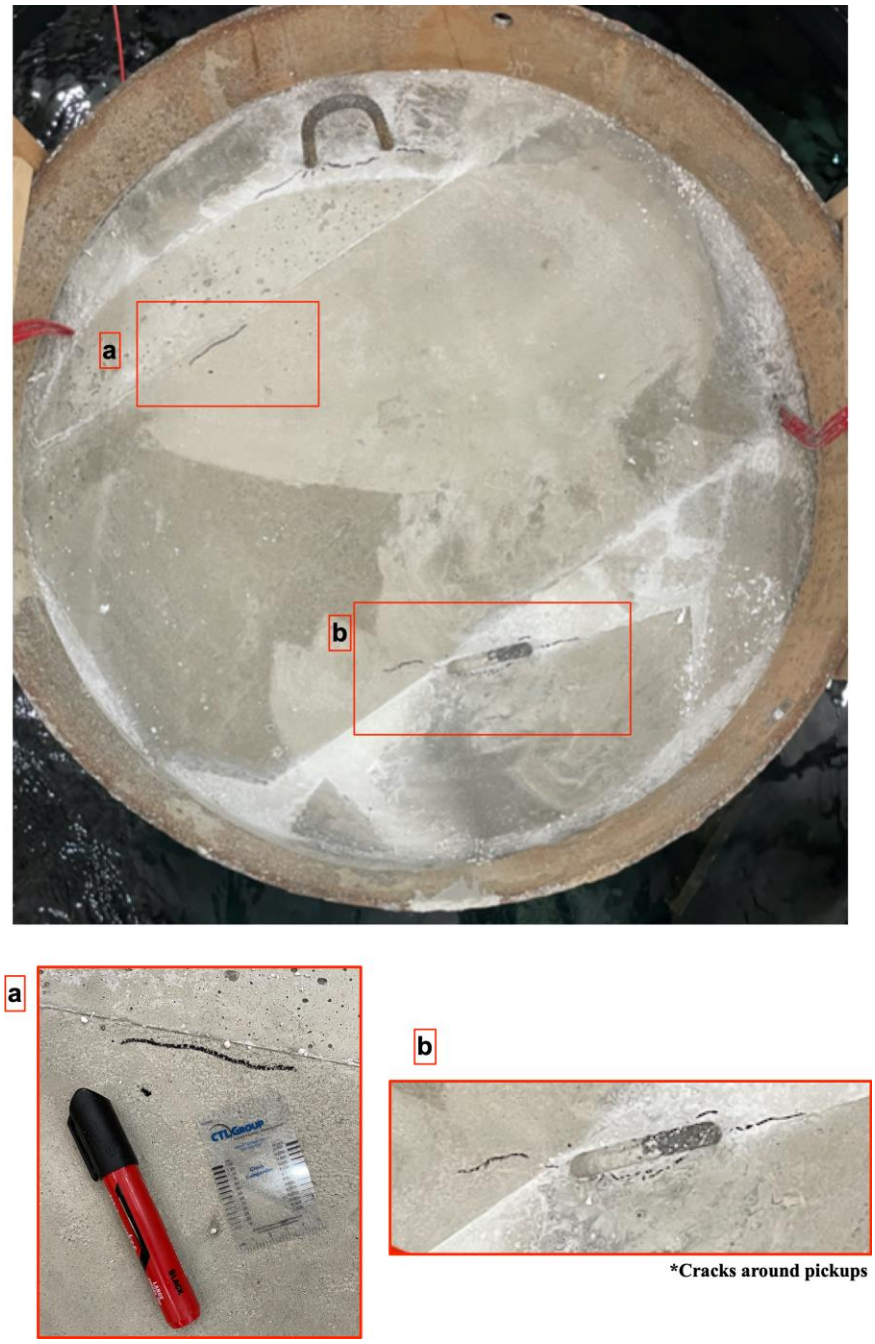

Figure 29. Photos. Cracking observed in Test S-W-A

DISCUSSION

Table 5 provides values from the maximum temperature differential and the maximum temperature differential per length for various points in the shaft. A summary of these results and results of other data from each of the five experiments are summarized in Table 4.

Table 3. Summary of results from laboratory testing.

Test:	C-A-A	C-S-A	C-W-A	S-W-B	S-W-A
Temperature Differential: Core and Surface (°F)	28.6	20.9	31.7	28.4	24.8
Temp. Differential per Length: Core and Surface (°F/in)	1.19	0.87	1.32	1.18	1.03
Temperature Differential: Core and 3” from Surface (°F)	19.6	18.9	29.9	25	22.1
Temp. Differential per Length: Core and 3” from Surface (°F/in)	0.93	0.9	1.42	1.19	1.05
Temperature Differential: Core and 6” from Surface (°F)	15.1	15.1	20.7	18.2	16.6
Temp. Differential per Length: Core and 6” from Surface (°F/in)	0.84	0.84	1.15	1.01	0.92
Temperature Differential: 3” from Surface and Surface (°F)	9.9	2.34	2.52	4.6	5.76
Temp. Differential per Length: 3” from Surface and Surface (°F/in)	3.3	0.78	0.84	1.53	1.92
Temperature Differential: 6” from Surface and Surface (°F)	15.1	7.2	11.2	11.2	10.8
Temp. Differential per Length: 6” from Surface and Surface (°F/in)	2.52	1.2	1.86	1.86	1.8
Temperature Differential: 9” from Surface and Surface (°F)	19.8	11.9	18.0	15.7	15.8
Temp. Differential per Length: 9” from Surface and Surface (°F/in)	2.2	1.32	2.00	1.74	1.76
Temperature Differential: 3” and 6” from Surface (°F)	5.22	4.86	9.72	6.9	6.12
Temp. Differential per Length: 3” and 6” from Surface (°F/in)	1.74	1.62	3.24	2.30	2.10
Temperature Differential: 3” and 9” from Surface (°F)	8.64	9.72	16.74	11.9	11.34
Temp. Differential per Length: 3” and 9” from Surface (°F/in)	1.44	1.62	2.79	1.98	1.89
Temperature Differential: 6” and 9” from Surface (°F)	5.22	6.12	7.02	5.2	5.4
Temp. Differential per Length: 6” and 9” from Surface (°F/in)	1.74	2.04	2.34	1.73	1.8

Table 4. Summary of results from laboratory testing.

Test:	C-A-A	C-S-A	C-W-A	S-W-B	S-W-A
Average Surrounding Air/Soil/Water Temperature (°F)	84.6	82.3	76.4	50.3	51.2
Circumferential Cracking	Yes	No	Yes	Yes	No
Maximum Crack Size (in)	0.03	0.01	0.03	0.02	0.02
Average Crack Size (in)	0.02	0.005	0.02	0.02	0.002
Number of cracks (H, M, L, N)*	H	L/N	H	M	L/N
Maximum Core Temperature (°F)	145.2	142	136.8	83.3	78.4
Maximum Core to 3” Differential (°F)	19.6	18.9	29.9	25	22.1
Maximum Differential per Length (°F/in)	3.3	2.04	3.24	2.30	2.04
Location of Maximum Differential per Length	Surface and 3”	6” and 9”	3” and 6”	3” and 6”	3” and 6”

*High, Moderate, Low, None based on relative visual inspection

All the specimen experienced some cracking. The test in air (C-A-A) and the test in water with cardboard casing (C-W-A) experienced the most cracking. These two specimens were poured with the same mix on relatively hot days. The first test in steel casing with Mix B (S-W-B) had moderate cracking, but not as significant as the C-A-A and C-W-A tests. The cardboard casing in soil (C-S-A) and the steel casing in water with Mix A (S-W-A) had very little cracking. It should be noted that the mix of S-W-A was relatively cold (51.2°F) on the day of the pour.

Current ACI and GDOT specifications limit the maximum temperature to 165°F and 158°F, respectively. Comparing the data generated from the experiment, none of the specimens reached the maximum temperature at the core and multiple specimens had noticeable cracking.

Current ACI and GDOT specifications both limit the maximum temperature differential between exterior and interior points to 35°F. Comparing the data generated from this

research shows that none of the specimen reached 35°F. The maximum differential was in 29.9°F for the specimen with cardboard Sonotube casing in water (C-W-A). This specimen experienced the most amount of cracking of the five. Interestingly, this ACI metric does not currently include the length over which the temperature change occurs. Consider the case of the first test, (C-A-A) where the internal temperature was calculated at the core. For determining the differential, one of three locations could likely be considered external: surface, 3 in from the surface, and 6 in from the surface. From these three cases, the differential would be calculated to be 28.8°F, 19.6°F, and 15.1°F, respectively. This is a very large difference to try to compare with one differential temperature cutoff. Further, these differentials do not predict potential cracking stresses in the newly placed concrete.

To address this, the researchers studied the temperature differentials per length between various locations. In the two cases with the highest amount of cracking, the temperature differentials per length were above 3.0 °F/in and both occurred within the exterior six inches. For the case with moderate level of cracking, the differential per length was 2.3 °F/in and occurred within the first six inches. Finally, the two cases with low/none cracking had differential per length of 2.04 °F/in and occurred within the first exterior six inches. From this data, the temperature differential per unit length of the first exterior six inches was the best predictor of amount of crack formation. This temperature differential appears to cause tensile stresses resulting in cracking. It was not the maximum temperature, but rather the differences in temperatures over a short distance which resulted in cracking – the mass concrete effect.

CHAPTER 5. COMPUTATIONAL MODELING

To better understand the behavior of shafts of different geometry and boundary conditions, a computational modeling effort was conducted. Multiple numerical modeling computer programs were explored (e.g., ConcreteWorks V2.0, COMSOL Multiphysics, DIANA) as possible software options because all had early age concrete modeling components. However, after a detailed investigation into the program, B4Cast was chosen due to its wide range of input possibilities and its 3D modeling capabilities. In addition, B4Cast's ability to model the necessary thermal properties and boundary conditions made it an ideal program to use for the thermal analysis of early-age mass concrete shafts.

B4Cast uses a linear flow analysis to model the temperature distribution over time within hydrating concrete. The temperatures were modeled by combining the heat of hydration, thermal heat capacity, thermal conductivity, and external environmental inputs. The concrete temperature versus time was extracted as output from the model.

MODEL PARAMETERS

This section details the multiple model parameters used in the B4CAST models of the field monitoring and laboratory efforts.

Heat of Hydration

The temperature change within early age concrete is largely due to the heat produced during the chemical reaction in cement hydration. B4Cast has two options for modeling the heat of hydration in the concrete: a direct input method and a data-model method. The

direct input method uses the direct relationship between the rate of the heat of hydration and the degree of hydration as the input. The data-model method allows the user to model the heat production rate as a function of the temperature and the current time. This study used this method due to its flexibility in modeling various concrete mix proportions. The heat of hydration is based on the powder content, which in the mix design was equal to 700 lb/yd^3 (with 210 lb/yd^3 of cement and 490 lb/yd^3 of slag).

Thermal Properties

Two fundamental equations govern the flow of temperature throughout a three-dimensional object: the three-dimensional extension of Fourier's law of conduction assuming thermal conductivity is isotropic and homogeneous and the increase of internal energy.[11]

The two critical thermal properties that govern the heat flow within the concrete, aside from the internal heat generation caused by cement hydration, are its thermal conductivity and its specific heat. Thermal conductivity is the rate of heat flow through a unit area under a unit temperature gradient or the ability of the material to conduct heat.[12-13] Conversely, the specific heat is the amount of heat required to raise the temperature per unit mass one degree. When specific heat is multiplied by the concrete density, it becomes the thermal heat capacity per unit volume.

In this research, the thermal conductivity of concrete was computed using the thermal conductivity values of the concrete constituents from *Concrete* and their volumetric fraction (2.76 W/m-K), which included the presence of a high percentage of cement replacement with slag.[14] The result closely matches the ACI 207 values of

2.6–2.7 W/m-K for concrete with granite aggregate. The concrete diffusivity was then taken to be 0.004 m^2/hr from the ACI 207 value for the granite aggregate. The conductivity and heat capacity values for other materials (e.g., Sonotube, plywood, steel forms) were chosen based on typical values as shown in Table 5.

Table 5. Material thermal properties.

Material	Thickness in (m)	Conductivity W/mK (kJ/mhC)
Sonotube	0.5 (0.013)	0.2 (0.72)
Insulation (polystyrene)	2 (0.051)	0.035 (0.126)
Water	30 (0.75)	0.598 (2.153)
Soil	30 (0.75)	2.55 (9.81)

Boundary Conditions

The external environmental conditions were modeled by way of boundary elements on the outside surface of the model. The wind effects were not modeled through a forced convection term associated with the boundary elements to model the heat lost to the environment by an exposed surface. The convection coefficient was modeled based on the actual ambient temperature for each shaft tested in the laboratory and from local historical weather data for shaft cast on site. However, the formwork and insulation initial temperatures were based on the average ambient temperature recorded before casting the concrete.

MODELING PROCEDURE

The detailed procedure used to model the shafts is given in Appendix E. An example of the B4Cast interface is given in Figure 30. The analysis focused on the first 100 hours of

the initial curing. This time frame matches the available data from laboratory experiments and field monitoring. All specimens and simulations reached their peak temperature within the first 100 hours. In the location where the peak temperature was reached, the full temperature profile at that time was analyzed to monitor the temperature gradient. As expected, the heat generation and the thermal conductivity were the two key parameters that affected the model the most. Specifically, the first influenced the maximum temperature in the center of the shaft, whereas the second influenced the temperature distribution from center (T_0) to edge (T_e).

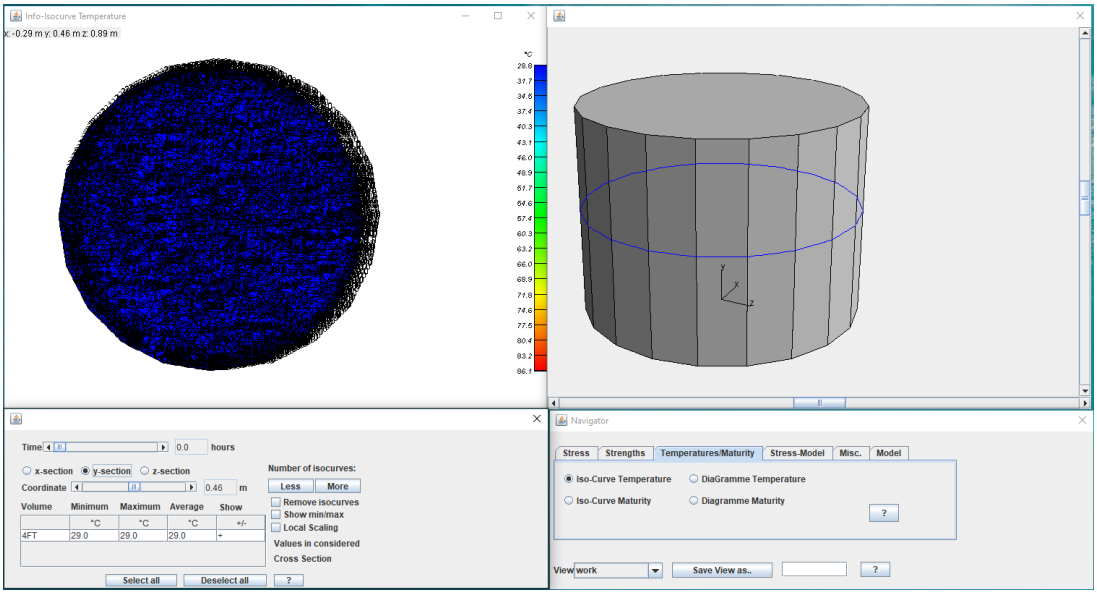

Figure 30. Model. B4Cast interface with shaft results.

MESH SENSITIVITY STUDY

A mesh sensitivity analysis was conducted to determine the largest mesh size that can return accurate results. In general, if the mesh is too coarse, isolines are not smooth. In that case, the structure needs to be re-meshed with a smaller element size. The mesh was studied in a range from 0.02 m to 0.2 m, as shown in Figure 31. The results of this study are given in Table 6. In this range, temperature differences were in the order of 0.05%

with smooth isolines. Therefore, a course mesh was then selected to optimize computing time. Specifically, a coarse mesh size of approximately 0.2 m was used.

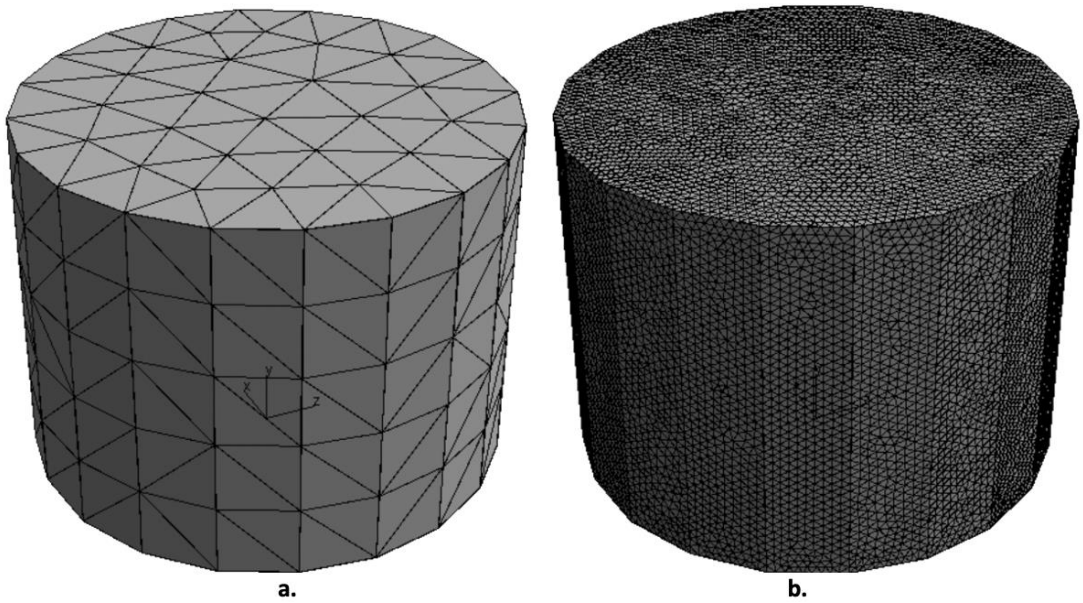

Figure 31. Model. Mesh sensitivity: a.) 0.2 m and b.) 0.02 m element size

Table 6. Mesh sensitivity analysis in a 4-foot diameter shaft.

Element size [m]	**Point distance from the center [in]**							
	0	6	9	12	15	18	21	24
0.02 (fine)	67.14	66.62	65.90	64.04	63.72	61.00	59.22	56.87
0.2 (coarse)	67.20	66.58	65.79	64.78	63.22	61.20	59.06	56.16
% Difference	0.001	0.001	0.002	0.011	0.008	0.003	0.003	0.013

MODEL CALIBRATION

Using the procedure in Appendix E, the model was calibrated with the laboratory experiments. Results from the models are given in Table 7. The results from the analytical models are within 5% of the experiments.

Table 7. Comparison between laboratory and B4Cast model.

Boundary	Type	T_0 [F]	T_e [F]	$T_0 - T_e$ [F]
Air	Lab	145	117	28
	Model	143	109	34
Water	Lab	137	105	32
	Model	143	113	30
Soil	Lab	142	123	19
	Model	149	122	27

PARAMETRIC STUDY

A parametric study was conducted to evaluate the temperature profiles of shafts of different diameters. In each diameter, three boundary conditions were considered: air, water, and soil. The results of these analyses are given in Figure 32, Figure 33, and Figure 34, respectively, with a summary given in Table 8.

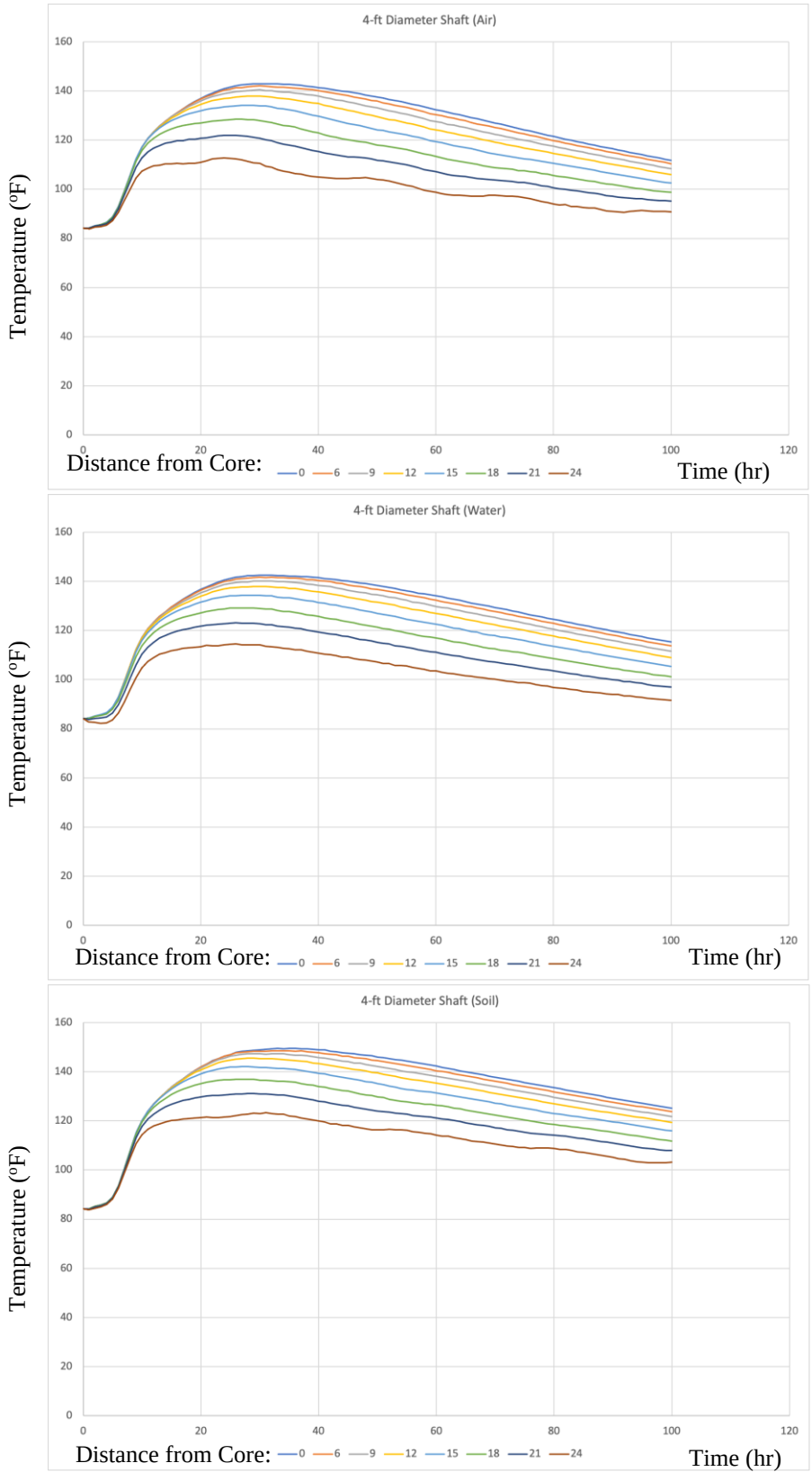

Figure 32. Graphs. Temperature profile for 4-ft diameter shafts

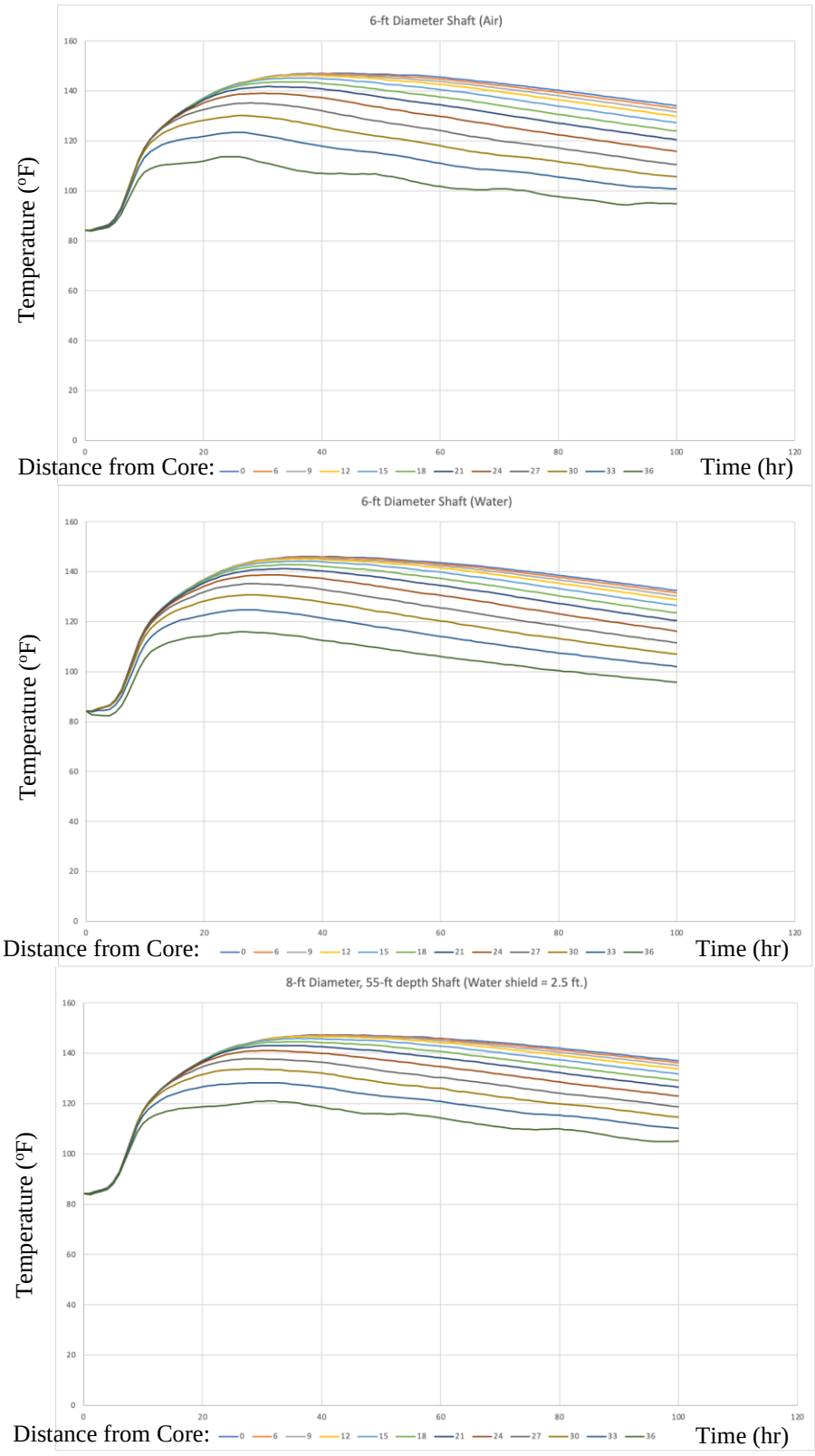

Figure 33. Graphs. Temperature profile for 6-ft diameter shafts

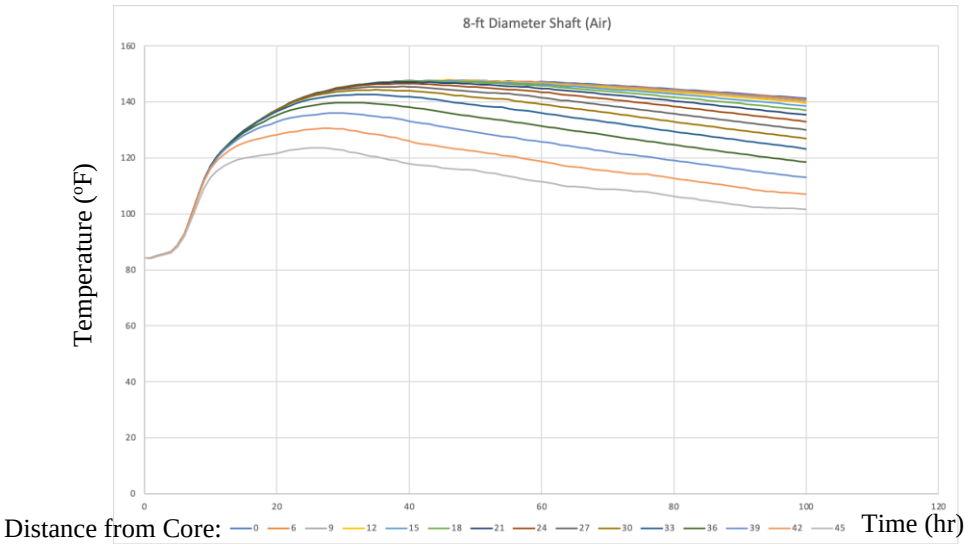

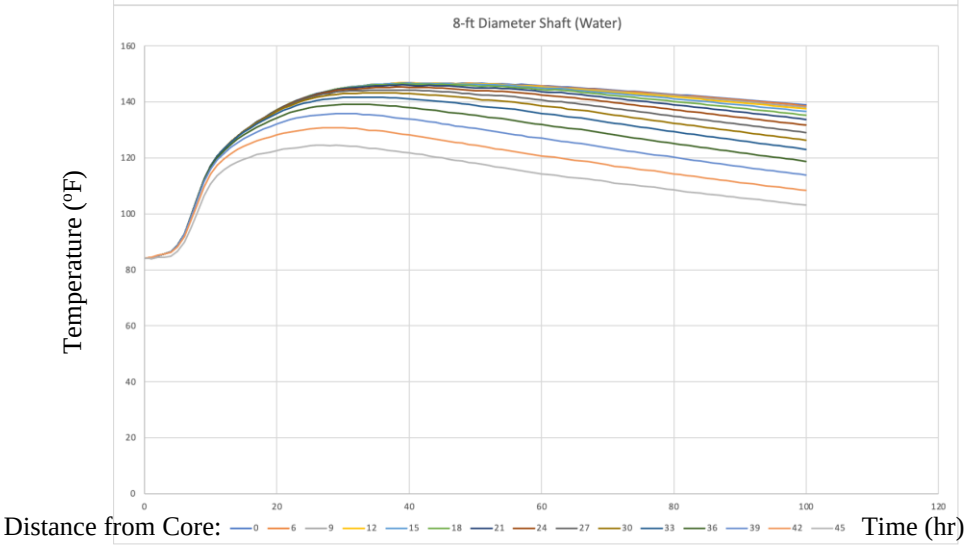

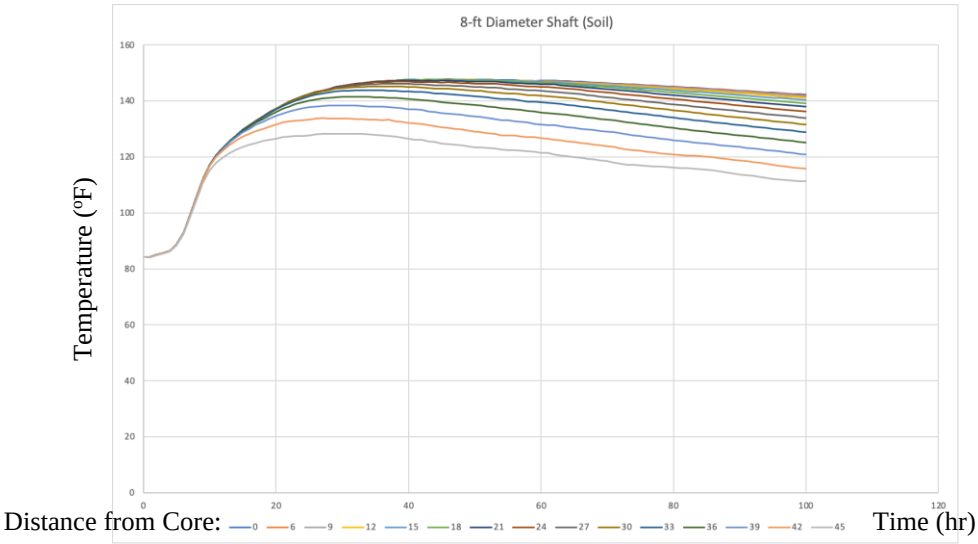

Figure 34. Graphs. Temperature profile for 8-ft diameter shafts

Table 8. Summary of temperature profiles.

Shaft Diameter	**Boundary Condition**	**Distance from the Center [in]**															
[ft]		0	6	9	12	15	18	21	24	27	30	33	36	39	42	45	$T_0 - T_e$
4	air	143	142	140	138	134	128	120	109								34
	water	143	142	140	138	134	128	120	109								34
	soil	150	149	147	145	141	136	130	122								28
6	air	147	147	146	146	144	142	140	136	130	124	117	107				40
	water	146	146	145	145	144	142	140	138	133	128	122	113				33
	soil	147	147	147	146	145	144	142	139	135	131	125	117				30
8	air	148	148	148	148	148	147	147	146	144	143	140	136	131	124	116	31
	water	147	147	147	147	147	146	146	145	144	143	141	138	134	128	122	25
	soil	148	148	148	148	148	148	147	147	146	144	143	140	136	131	125	23

DISCUSSION

The influence of the edge conditions in the shaft's early-age temperature development is like what was observed in field monitoring. Figure 35 shows a plan view of the shaft location in the Martin Luther King Junior Boulevard bridge over the Ocmulgee River, located in Bibb County, GA. The attention is on three shafts (Bent 2 Caisson 3, Bent 3 Caisson 3, and Bent 4 Caisson 2.) For these shafts, the temperature development in the first 100 hours is reported in Figure 36, where series 1 and 2 show the curve for the data collected at the top of the shaft, series 3 and 4 in the middle, and series 7 and 8 at the bottom.

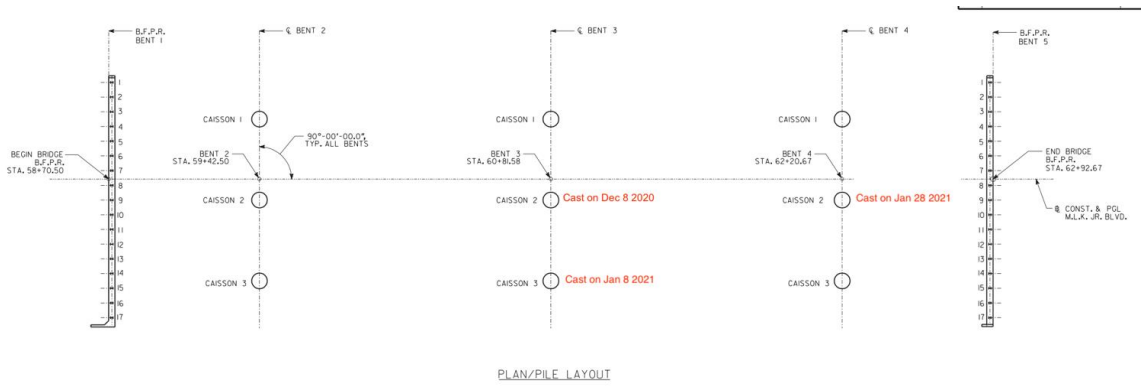

Figure 35. Schematic. Location of field monitored shafts. Bent 2 Caisson 3 (partially water and soil), Bent 3 Caisson 3 (water), Bent 4 Caisson 2 (soil)

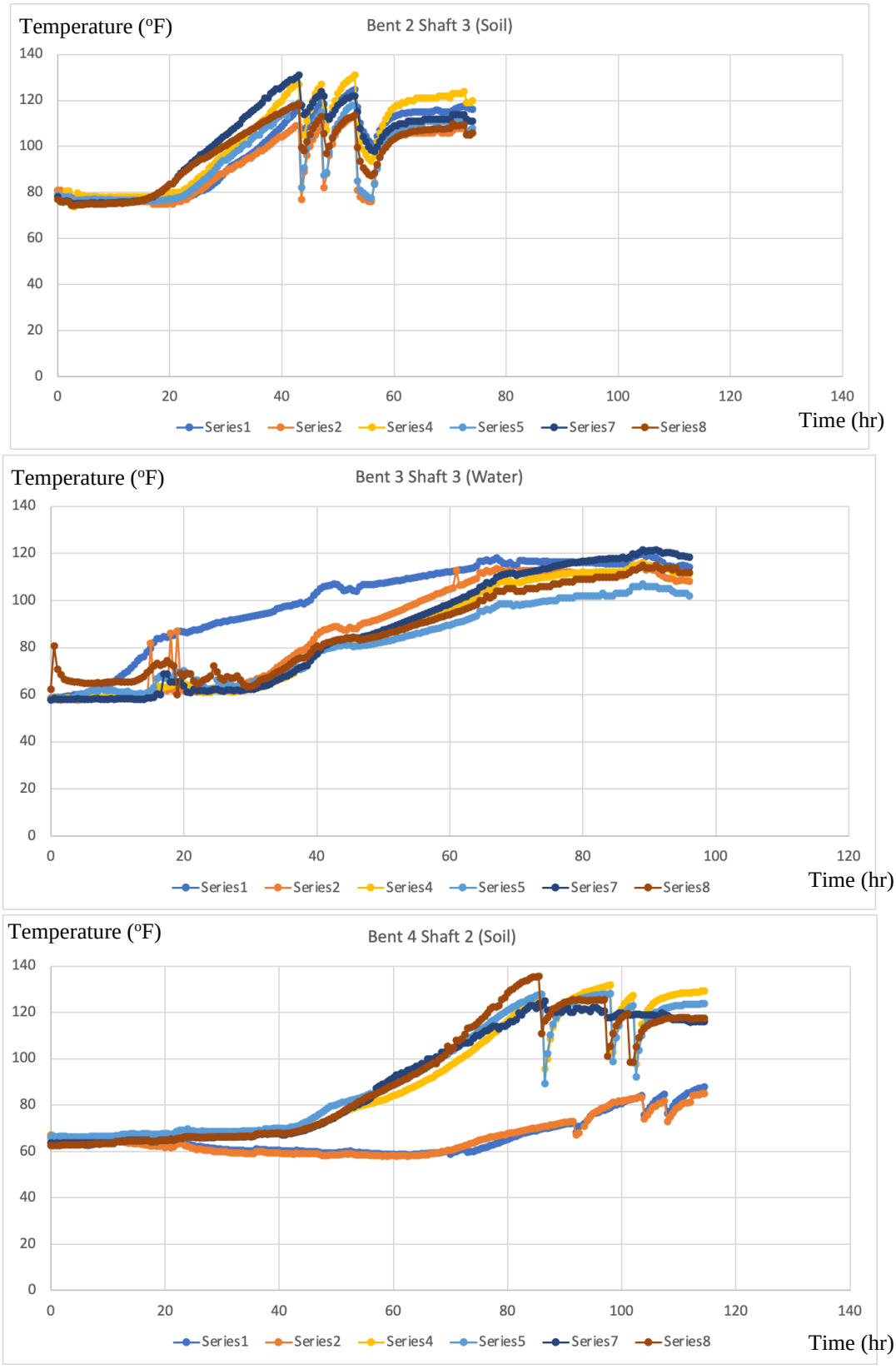

Figure 36. Graphs. Temperature (F) development in field monitored shafts

It can be observed that for Bent 2 Caisson 3 and Bent 4 Caisson 2, as the shafts were rapidly increasing the internal temperature (approaching 140 °F), the cooling system was activated three times to avoid the generation of mass concrete phenomena. Boundary conditions were soil in both shafts. Conversely, in the case of the water-immersed Bent 3 Caisson 3, the active cooling system was never operated because the internal temperature never reached critical values. In all cases, the shafts were only monitored at the center of the cross section.

A simulation for a shaft with similar geometry (8-ft diameter and 55-ft length) and similar boundary conditions (soil and water) is reported in Figure 37 and summarized in Table 9. The overall trend is like that observed in the field monitoring with higher peak temperatures in soil-immersed shafts. However, it can be observed that the temperature gradient in the shaft submerged in water is more significant, leaving the possibility open for possible crack formation at the edge of the shaft.

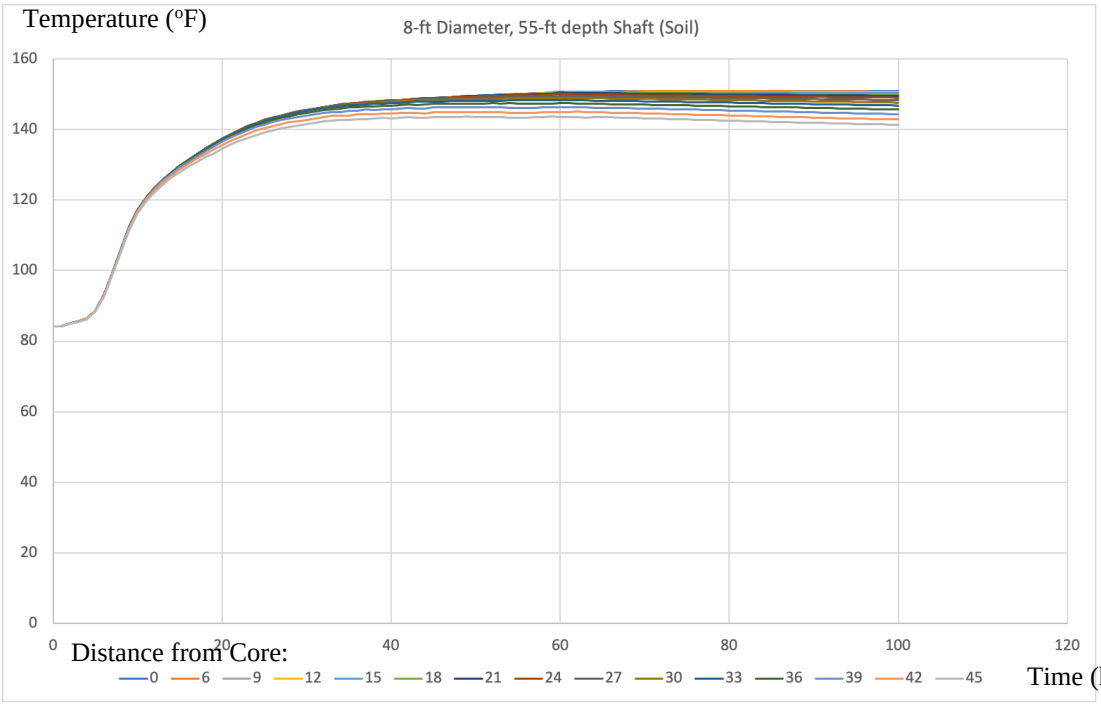

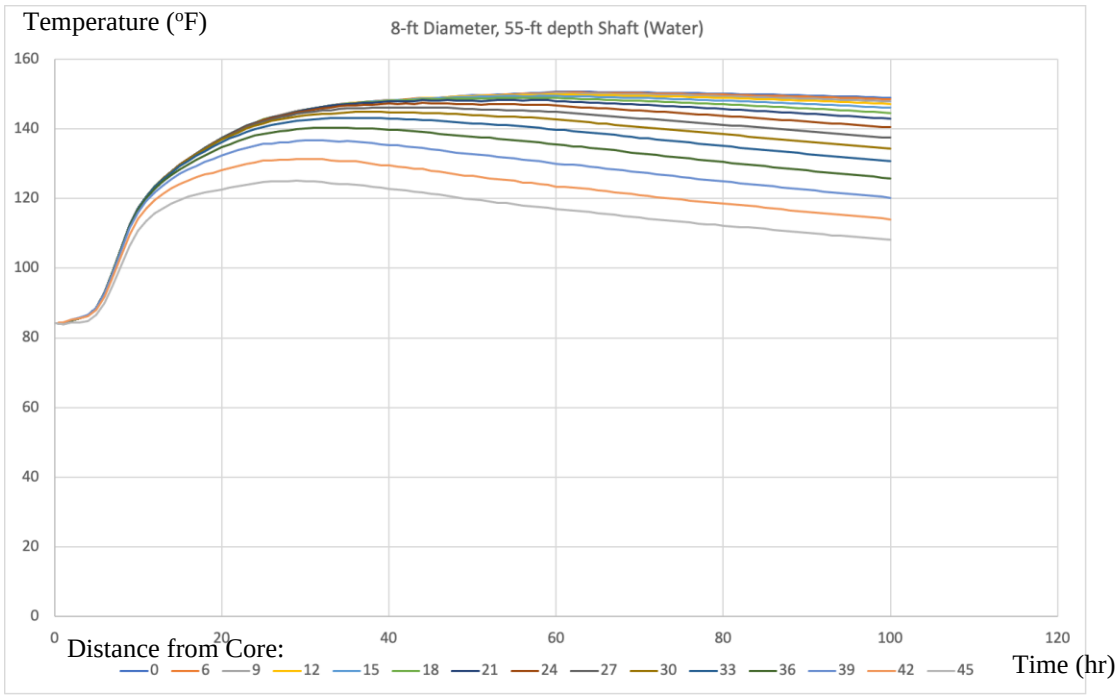

Figure 37. Graphs. Simulated temperature profiles for 8-ft diameter shaft in soil and water.

Table 9. Summary of temperature profiles for 8-ft shaft in soil and water

Shaft Diameter	Boundary Condition	Distance from the Center [in]															
[ft]		0	6	9	12	15	18	21	24	27	30	33	36	39	42	45	$T_0 - T_e$
8	soil	151	151	151	151	150	150	150	149	149	148	148	146	145	144	142	9
8	water	151	150	150	150	149	149	148	146	145	142	140	135	130	123	117	34

CHAPTER 6. CONCLUSION AND RECOMMENDATIONS

This research project explored the effects of shaft diameter and boundary condition on mass concrete behavior using a combined field monitoring, laboratory testing, and modeling effort. The main technical conclusions from the research project are as follows:

1. In the field monitoring of eight-foot diameter shafts of the same mix design, the shaft surrounded by water did not reach a high enough maximum temperature to activate the internal cooling system based on contractor monitoring at the center of the diameter of shaft. The shafts in soil reached the prescribed temperature (140 ^{o}F) and the cooling system was activated.
2. Laboratory experiments were conducted to understand the effects of boundary condition on the shaft performance. Five shafts were tested with air, water, and soil boundaries with cardboard and steel casings. Temperatures were monitored at multiple locations along the diameter, including the edges of the shafts. In three of the cases, significant cracking was observed in each specimen at the location of the longitudinal reinforcement. Very little cracking was observed in the soil specimen or in the water specimen for which concrete was placed on the coldest day. None of the specimens reached a maximum core temperature or temperature differential to meet current ACI or GDOT mass concrete specifications.
3. An analysis was conducted on the laboratory data to quantify the temperature gradient per unit length at the edges. It was found that the temperature differential

per inch length in the first exterior six inches (up to location of reinforcement) was the best predictor of crack formation in the specimens.

4. A computational parametric study was conducted on shafts of different diameter and boundary conditions with the mix design used in the field and in the laboratory experiments. It was found that shafts up to eight feet in diameter did not reach the current maximum core temperature in current ACI or GDOT specifications. However, the temperature gradient at the edge of the shaft in water and air environment was much greater than in shafts with surrounding soil, even in small diameter sections.
5. Additional computational models with varying mix designs should be considered to generalize the above findings to all GDOT shafts.

The recommendations that could be incorporated into GDOT Specifications are as follows:

1. It is likely that shafts in soil with diameters greater than six feet with certain mass concrete mix designs do not need to be constructed with interior water-cooling pipes because their core temperature and gradient per inch length do not reach values near the ACI or current GDOT temperature specifications nor did they reach a differential per inch length that is indicative of cracking based on this research. The shaft in soil also did not exhibit cracking in the diameters that were tested in the laboratory.
2. Because the temperature gradient per unit length near the boundary condition can be significant in the cases where the shafts are in water and in air, it is recommended that monitoring at the shaft boundaries be the metric used for

turning on water-cooling. Alternatively, it could be more cost effective to remove the monitoring portion and simply turn on the water in all cases for shafts in water, since a water source would be nearby.

APPENDIX A: CONCRETE MIX

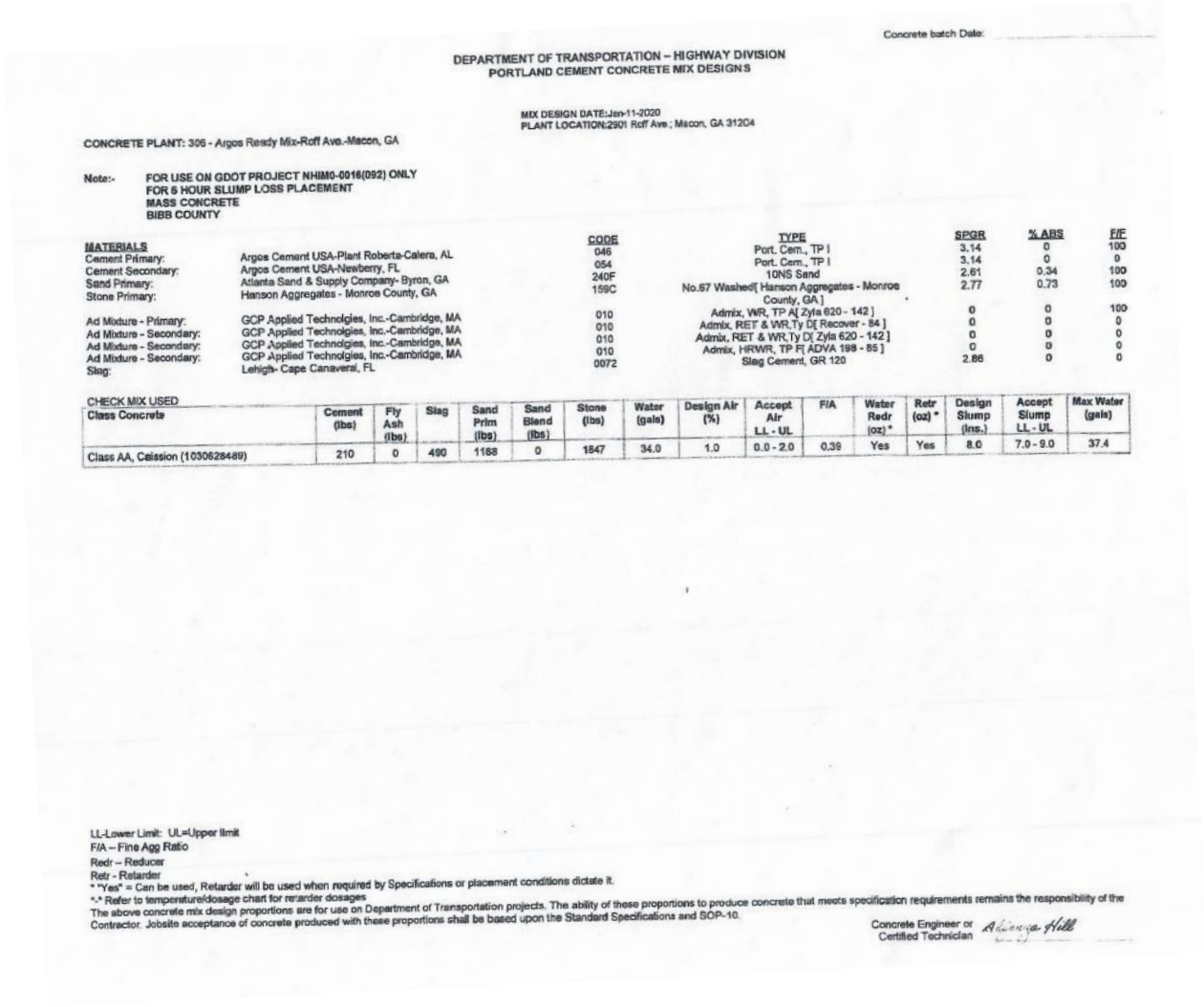

Concrete batch Date:

DEPARTMENT OF TRANSPORTATION – HIGHWAY DIVISION
PORTLAND CEMENT CONCRETE MIX DESIGNS

MIX DESIGN DATE:Jan-11-2020
PLANT LOCATION:2901 Roff Ave.; Macon, GA 31204

CONCRETE PLANT: 306 - Argos Ready Mix-Roff Ave.-Macon, GA

Note:- FOR USE ON GDOT PROJECT NHIM0-0016(092) ONLY
FOR 6 HOUR SLUMP LOSS PLACEMENT
MASS CONCRETE
BIBB COUNTY

MATERIALS		CODE	TYPE	SPGR	% ABS	F/F
Cement Primary:	Argos Cement USA-Plant Roberta-Calera, AL	046	Port. Cem., TP I	3.14	0	100
Cement Secondary:	Argos Cement USA-Newberry, FL	054	Port. Cem., TP I	3.14	0	0
Sand Primary:	Atlanta Sand & Supply Company- Byron, GA	240F	10NS Sand	2.61	0.34	100
Stone Primary:	Hanson Aggregates - Monroe County, GA	159C	No.67 Washed[Hanson Aggregates - Monroe County, GA]	2.77	0.73	100
Ad Mixture - Primary:	GCP Applied Technolgies, Inc.-Cambridge, MA	010	Admix, WR, TP A[Zyta 620 - 142]	0	0	100
Ad Mixture - Secondary:	GCP Applied Technolgies, Inc.-Cambridge, MA	010	Admix, RET & WR,Ty D[Recover - 84]	0	0	0
Ad Mixture - Secondary:	GCP Applied Technolgies, Inc.-Cambridge, MA	010	Admix, RET & WR,Ty D[Zyta 620 - 142]	0	0	0
Ad Mixture - Secondary:	GCP Applied Technolgies, Inc.-Cambridge, MA	010	Admix, HRWR, TP F[ADVA 195 - 85]	0	0	0
Slag:	Lehigh- Cape Canaveral, FL	0072	Slag Cement, GR 120	2.86	0	0

CHECK MIX USED

Class Concrete	Cement (lbs)	Fly Ash (lbs)	Slag	Sand Prim (lbs)	Sand Blend (lbs)	Stone (lbs)	Water (gals)	Design Air (%)	Accept Air LL - UL	F/A	Water Redr (oz) *	Retr (oz) *	Design Slump (ins.)	Accept Slump LL - UL	Max Water (gals)
Class AA, Caission (1030628489)	210	0	490	1188	0	1847	34.0	1.0	0.0 - 2.0	0.39	Yes	Yes	8.0	7.0 - 9.0	37.4

LL-Lower Limit: UL=Upper limit
F/A – Fine Agg Ratio
Redr – Reducer
Retr - Retarder
* "Yes" = Can be used, Retarder will be used when required by Specifications or placement conditions dictate it.
- Refer to temperature/dosage chart for retarder dosages
The above concrete mix design proportions are for use on Department of Transportation projects. The ability of these proportions to produce concrete that meets specification requirements remains the responsibility of the Contractor. Jobsite acceptance of concrete produced with these proportions shall be based upon the Standard Specifications and SOP-10.

Concrete Engineer or Certified Technician

Figure 38. Datasheet. Mix design A

Plant	: Atlanta		
Start Time	: 01/28/22 13:36:14	End Time	: 01/28/22 13:41:13
Product Code	: GT35267-1S	Destination	: Loadout
Load Size	: 3.00	Ticket	: 8434889
Truck No.	: 0443	Load Id	: 205173
Job	: 158	Customer	: GEORGIA TECH
Water Trim	: -5 gal	Moist. Water	: 24.99
Ideal W/C	: 0.4053	Acutal W/C	: 0.3392

MATERIAL	DESIGN	TARGET		ACTUAL		MST	ABS
HS	14.00	42.00	floz	41.00	floz	0.00%	
2100	21.00	63.00	floz	62.00	floz	0.00%	
WATER	34.00	62.15	gal	62.00	gal		
NATURAL SAND	1257.00	3978.41	lb	4000.00	lb	5.50%	0.00%
67 STONE	1798.00	5394.00	lb	5340.00	lb	0.00%	0.00%
SLAG	490.00	1470.00	lb	1510.00	lb		
TYPE I	210.00	630.00	lb	630.00	lb		

SCALE	START TARE	END TARE
AggLoadCell1	0 lb	0 lb
AggLoadCell6	-20 lb	0 lb
CemLoadCell1	15 lb	5 lb
WtrLoadCell1	0 gal	0 gal

Figure 39. Datasheet. Mix design B.

APPENDIX B: FIELD MONITORING SHAFT DRAWINGS

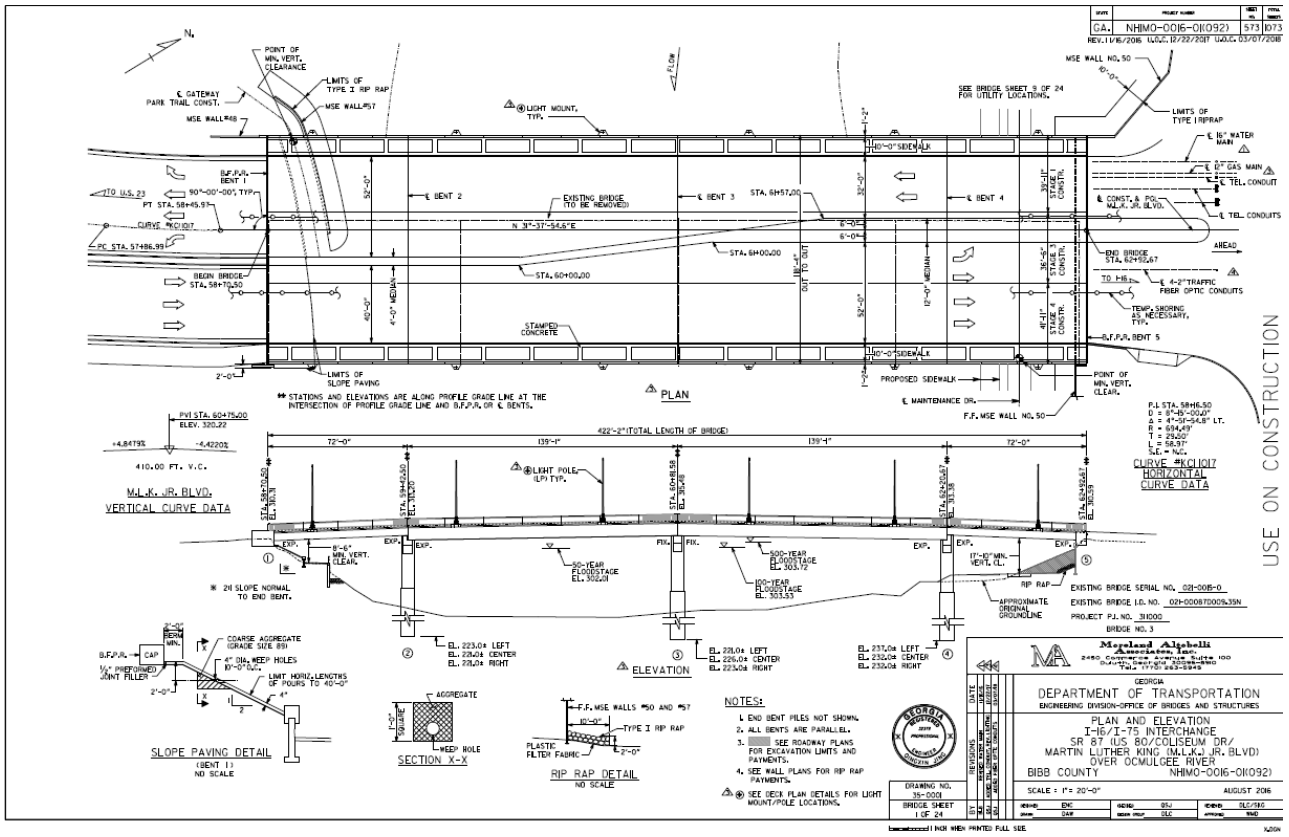

Figure 40. Engineering drawing. Field monitoring shaft drawing

APPENDIX C: RESULTS FROM FIELD MONITORING

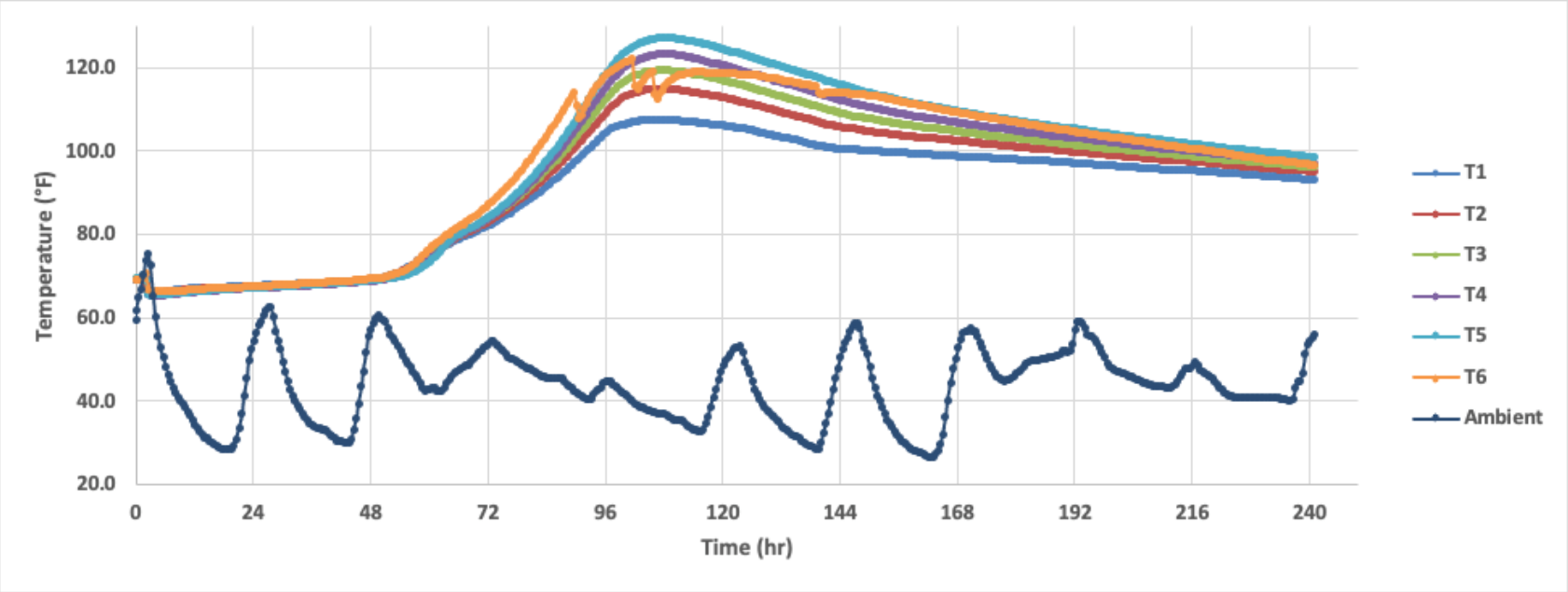

Figure 41. Graph. Field monitoring temperature data, gauges T1-T6

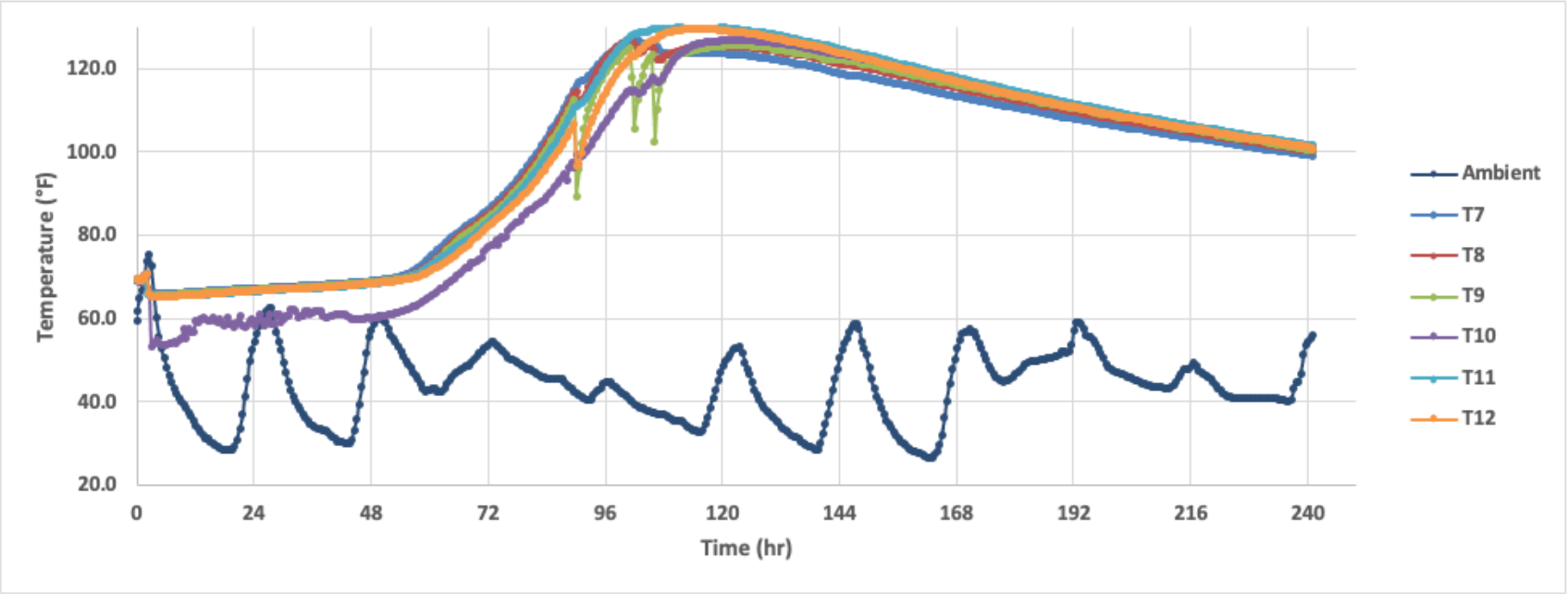

Figure 42. Graph. Field monitoring temperature data, gauges T7-T12

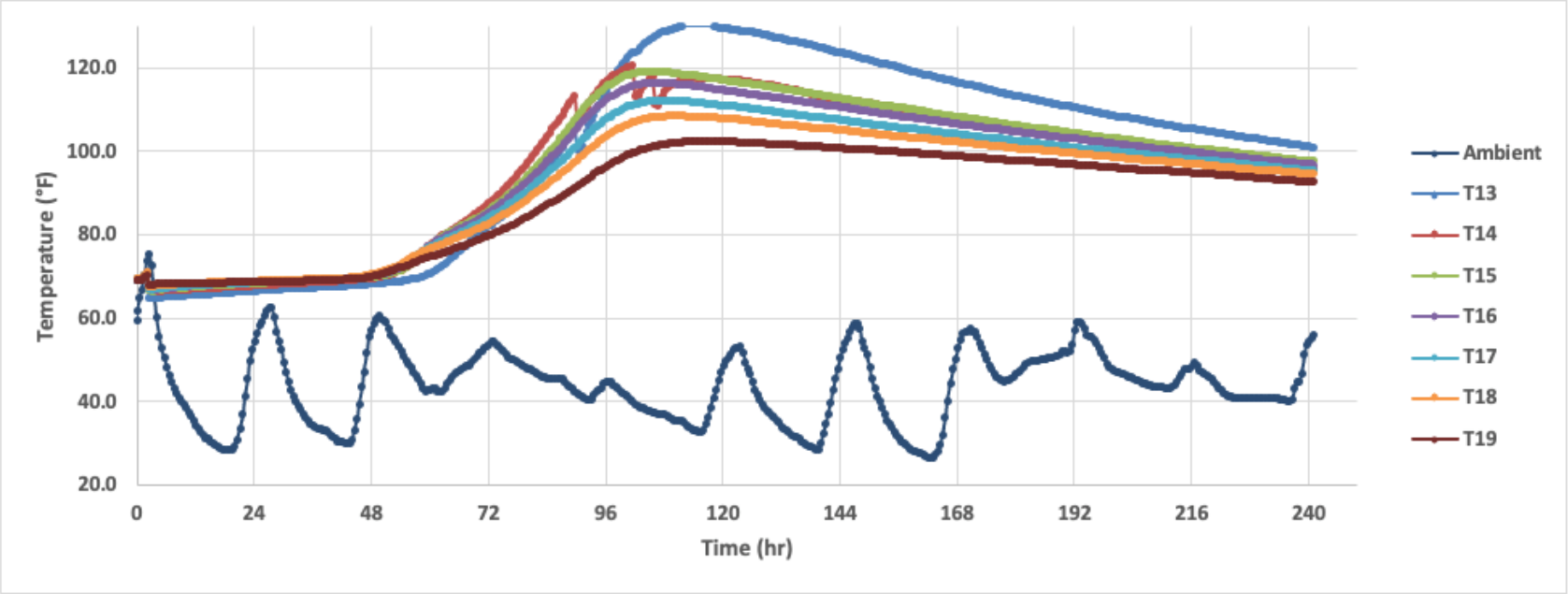

Figure 43. Graph. Field monitoring temperature data, gauges T13-T19

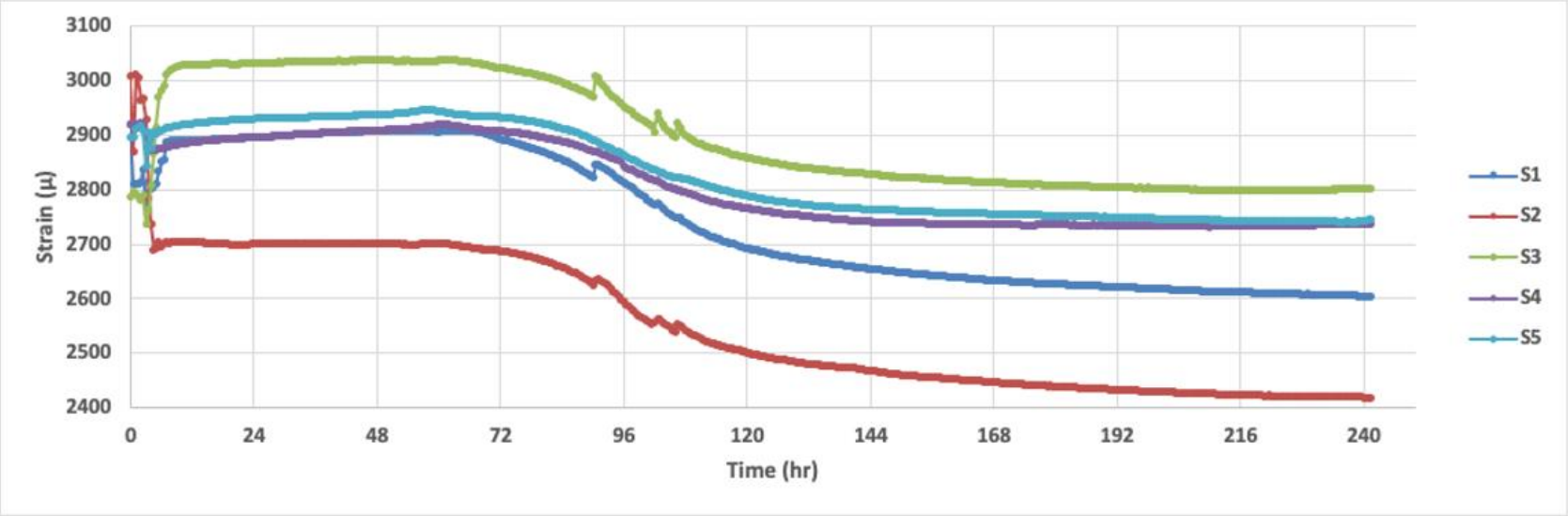

Figure 44. Graph. Field monitoring strain data

APPENDIX D: RESULTS FROM LABORATORY TESTS

This appendix contains the graphical temperature and strain results for each laboratory specimen. Also included are the properties for the concrete batches that were used for each specimen. The air specimen had its own batch, referred to as batch 20210716 while the water and soil specimens were the same batch, referred to as batch 20210823.

Table 10. Batch 20210716 properties determined from lab tests.

Batch 20210716		
3 Day Tests		
f'c	0.861	ksi
E	1672	ksi
7 Day Tests		
f'c	1461	ksi
28 Day Tests		
f'c	3.784	ksi
E	2785	ksi

Table 11. Batch 20210823 properties determined from lab tests.

Batch 20210823		
3 day		
f'c	2.00	ksi
E	2523	ksi
7 day		
f'c	3.22	ksi
28 day		
f'c	5.34	ksi
E	4590	ksi
9-day α_{avg}	0.00045	C^{-1}
28-day α_{avg}	0.00051	C^{-1}

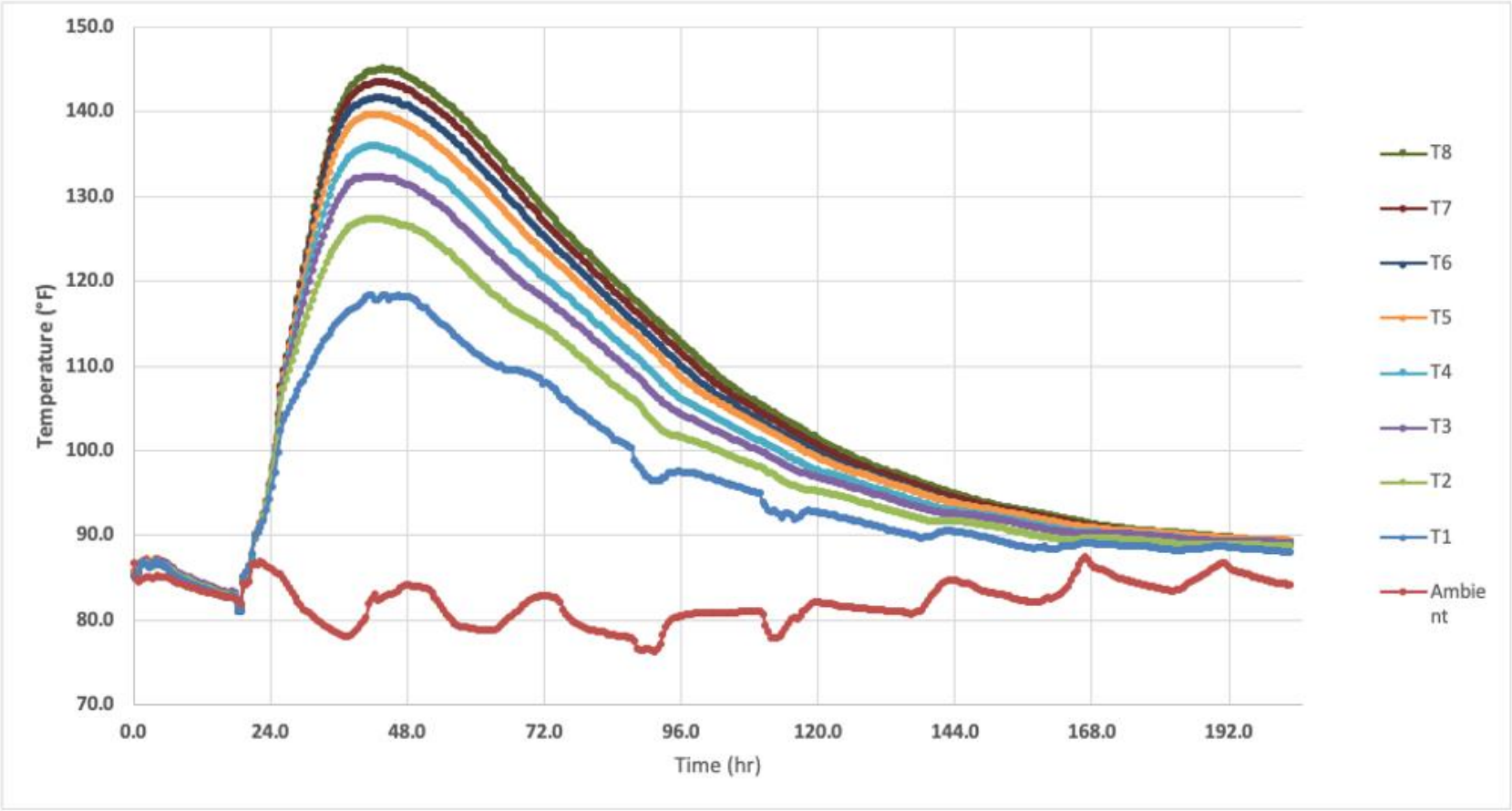

Figure 45. Graph. Test C-A-A temperature data, gauges T1-T8

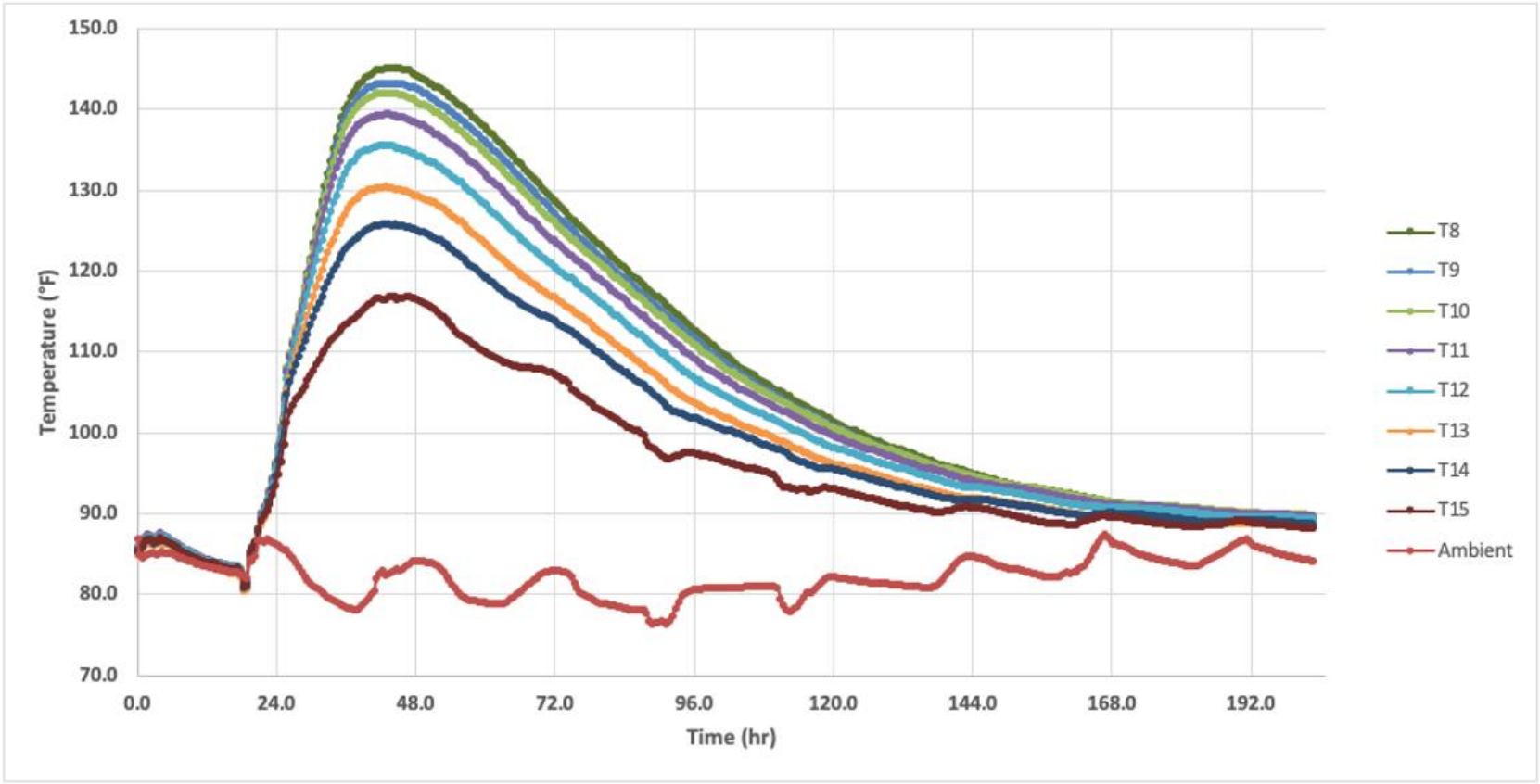

Figure 46. Graph. Test C-A-A temperature data, gauges T8-T15

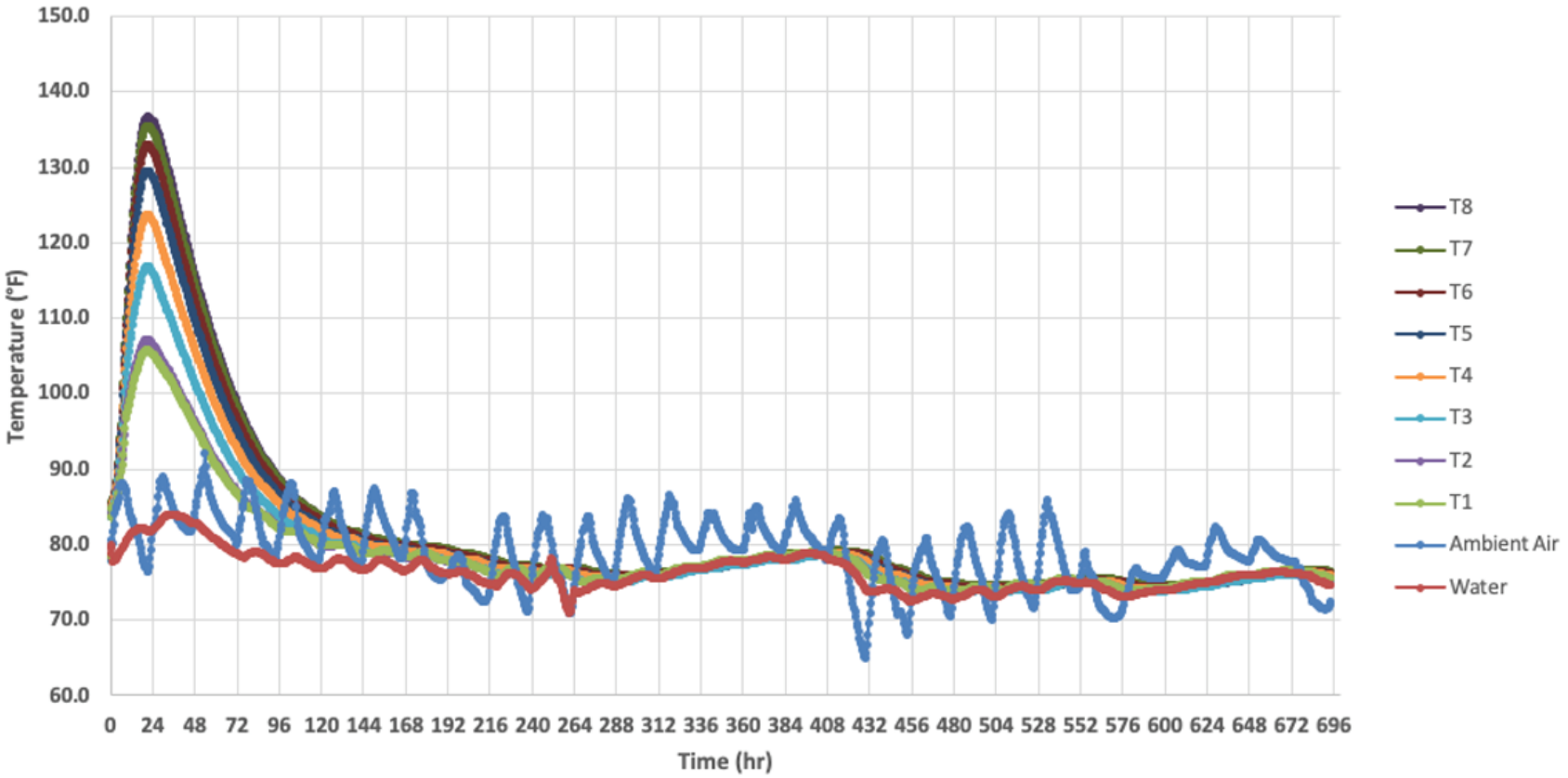

Figure 47. Graph. Test C-W-A temperature data, gauges T1-T8

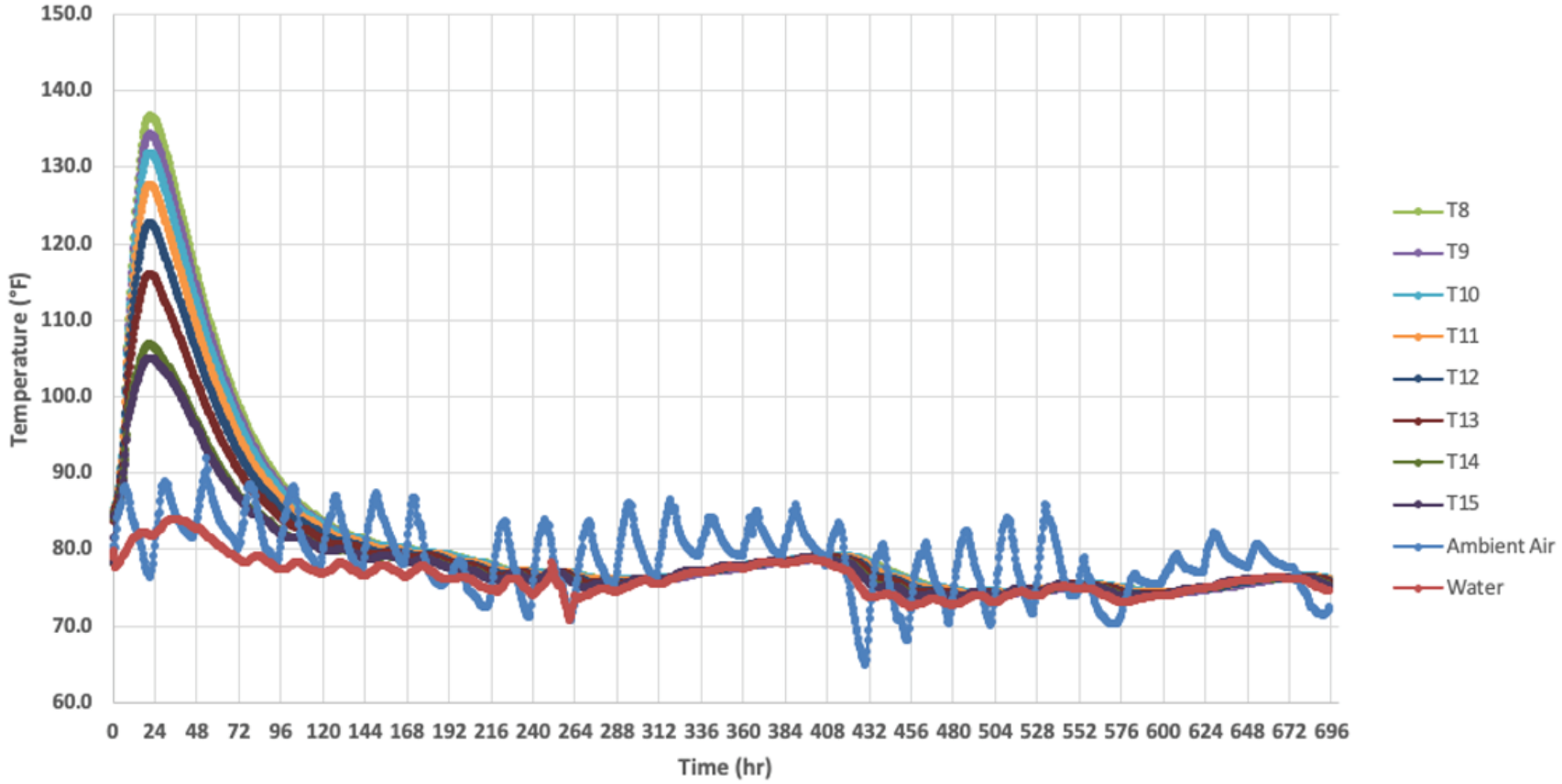

Figure 48. Graph. Test C-W-A temperature data, gauges T8-T15

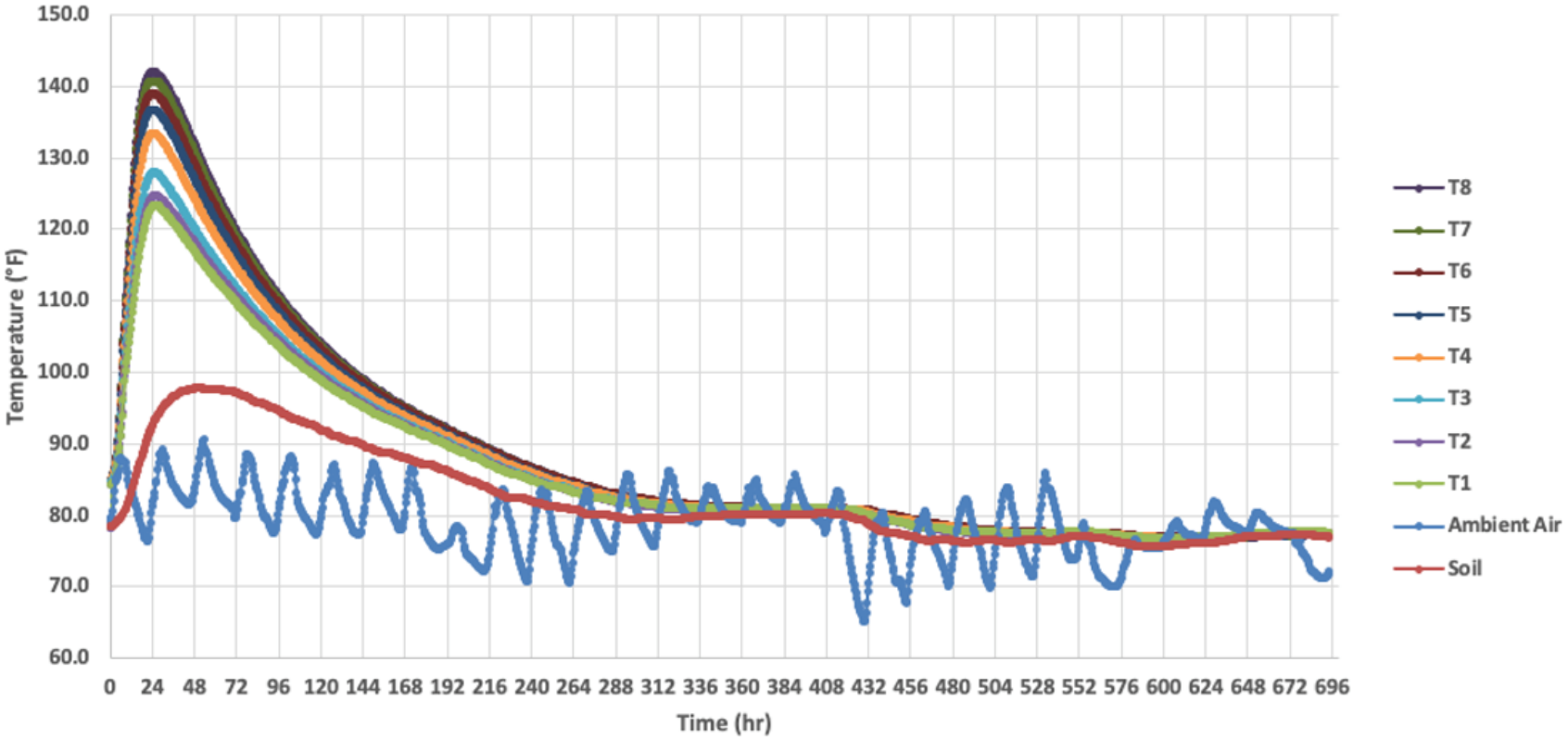

Figure 49. Graph. Test C-S-A temperature data, gauges T1-T8

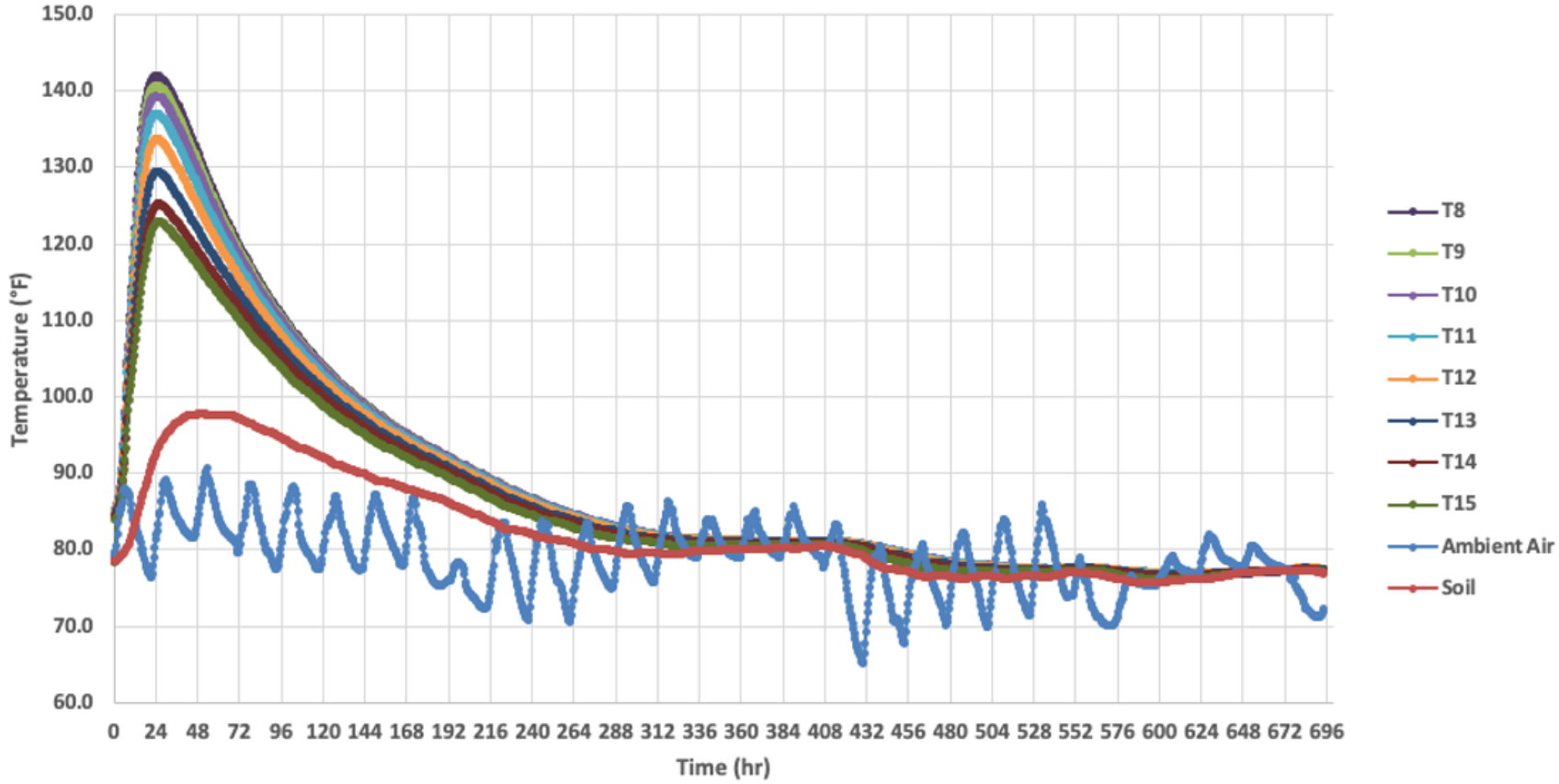

Figure 50. Graph. Test C-S-A temperature data, gauges T8-T15

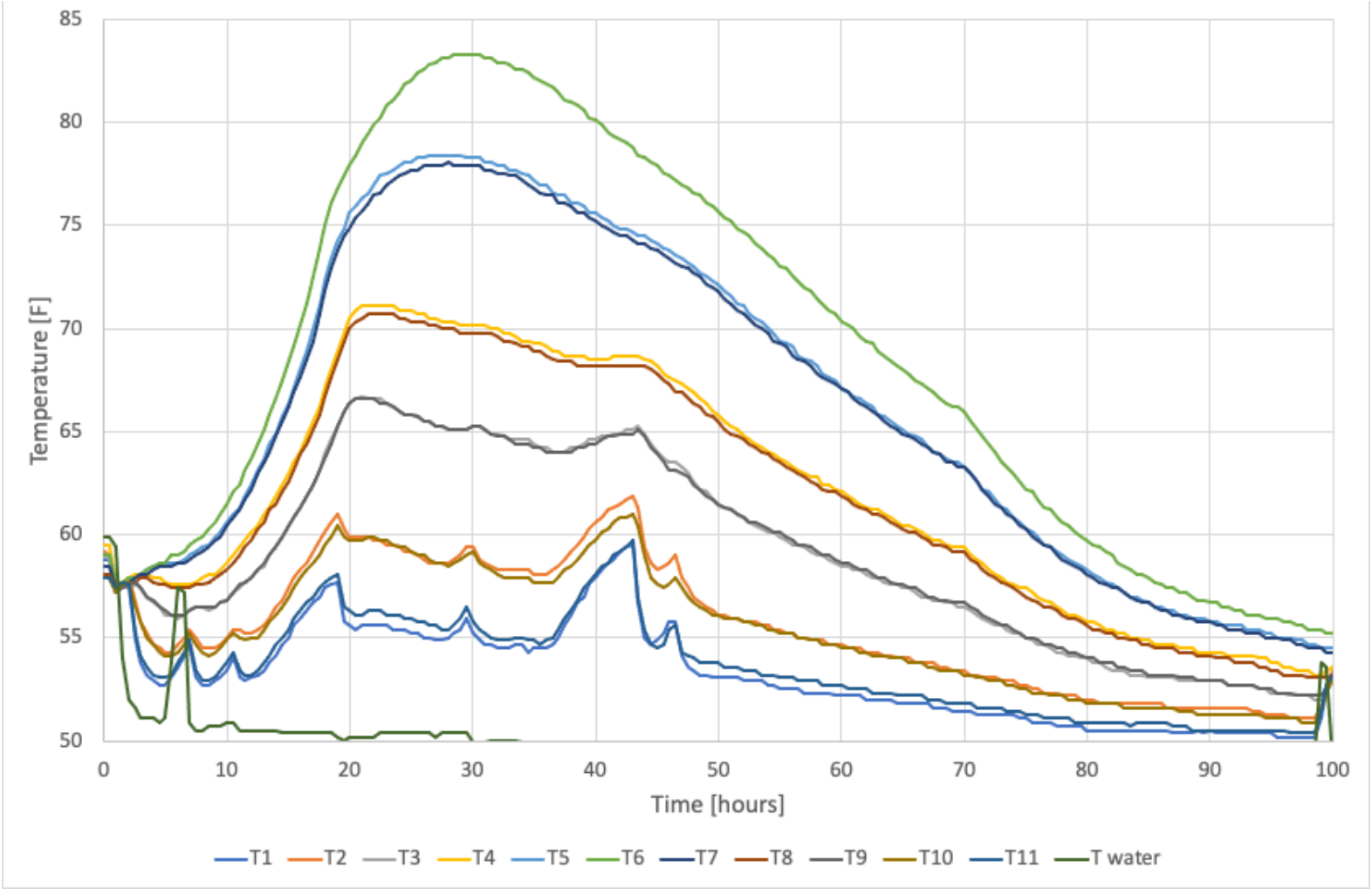

Figure 51. Graph. Test S-W-B temperature data

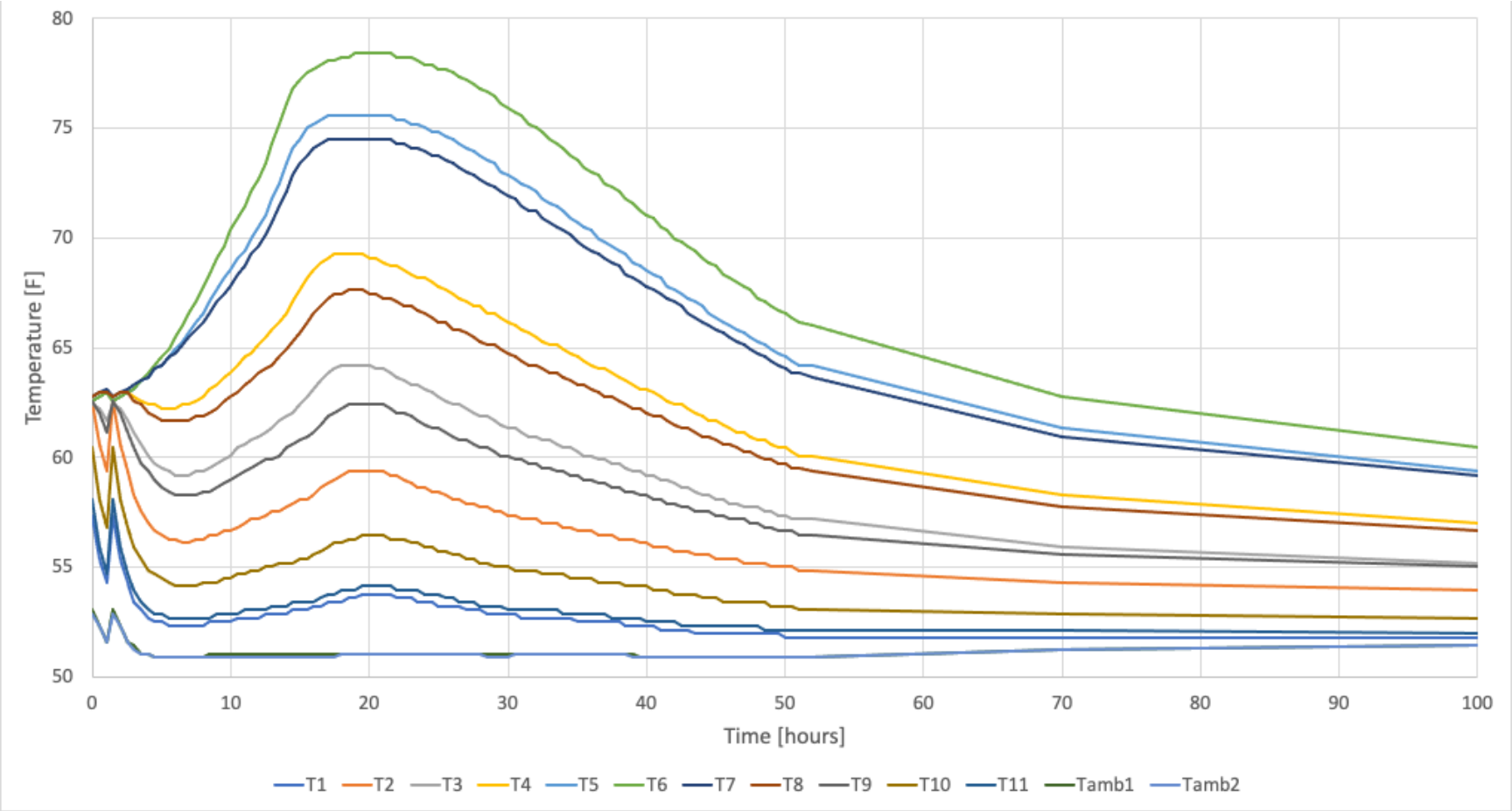

Figure 52. Graph. Test S-W-A temperature data

APPENDIX E: B4CAST MODELING PROCEDURE

Below is the simplified procedure that was used to model the shaft.

1. Define Geometry
    a. Define volume name
    b. Define Cross section
        i. New cross section
            1. Circle
            2. Radius
            3. Number or vertices
    c. Origin of (r,s,r)-system: 0.0, 0.0, 0.0
    d. T-vector: 0.0, 1.0, 0.0
    e. Direction point, P: 1.0, 0.0, 0.0
    f. Time of placing: 0
    g. Initial temperature: 29 C
    h. Initial maturity: 0.0
    i. Select material
        i. Load from library temporary material (it will be edited later)
        ii. Select Hetek
    j. Size of elements: 0.20 m (this parameter defines the sensitivity of the mesh)
    k. Press Apply and then OK to continue
2. Define Material
    a. Material Name: CONCSLAG
    b. Maturity based on Arrhenius: use default values
    c. Based on Powder: 415.3 kg/m^3
    d. Heat generation
        i. In the Development select Data-Model
        ii. Change the Heat Generation curve by importing Maturity and Value, use Load File (.txt can be imported) to modify the curve.
        iii. Heat Generation affects maximum temperature: 68 hours, 204 KJ/kg

e. Tensile, compression, and mechanical properties can be defined if data are available similarly to how the heat generation.

3. Apply the material. In the Volume section, the material CONCSLAG will now appear in the list. Select CONCSLAG, Apply, and then OK.
4. Boundary Conditions
    a. Convection Temperature. The temperature relation is used for the calculation of convective heat transfer together with the wind speed and the shield.
        i. Ambient temp (27.9 C is average over the duration of data collection for air sample)
        ii. Soil Temp (27.9 C is average over the duration of data collection)
        iii. Water Temp (24.6 C is average over time)
    b. Shield. A shield is a part of a thermal boundary. The shield is used for the calculation of convective heat transfer together with the wind speed and the convective temperature (i.e., sonotube, water, soil, air). Values are reported in Table 1.
    c. Wind. None.
5. Solving the model.
    a. Generate Mesh.
    b. Calculate Temperature
6. Exporting values.
    a. Use DiaGramme Temperature to export data in specific locations.
    b. Points were created from the center (0 in) to the edge (from 24 to 48 in) with 3 in of distance in-between points.

ACKNOWLEDGMENTS

The following individuals at GDOT provided many valuable suggestions throughout this study: Mr. Steve Gaston, Assistant State Bridge Construction Liaison; Mr. Jason Waters, Concrete Branch Chief; Mr. Chris Watson, Bridge Engineer; Ms. Sarah Lamothe, Research Program Manager; and Ms. Supriya Kamatkar, Assistant Office Head, Office of Performance-based Management and Research. The opinions and conclusions expressed herein are those of the authors and do not represent the opinions, conclusions, policies, standards, or specifications of GDOT or of other cooperating organizations.

The authors would like to thank the Mr. Jonathon Johnson for his assistance in the laboratory, and Mr. Jeremy Mitchell for his assistance in the laboratory experiment.

The authors express their profound gratitude to all these individuals for their assistance and support during the completion of this research project.

REFERENCES

1. ACI (American Concrete Institute). (2005). Guide to Mass Concrete. ACI 207.1R-05. Farmington Hills, MI: ACI.

2. ACI (American Concrete Institute). (2020). Report on Cooling and Insulating Systems for Mass Concrete. ACI 207.4R-20. Farmington Hills, MI: ACI.

3. ACI (American Concrete Institute). (2021). ACI Concrete Terminology. ACI CT-21. Farmington Hills, MI: ACI.

4. GDOT (Georgia Department of Transportation). (2014). Concrete Structures. GDOT SSP 500. Atlanta, GA: GDOT.

5. GDOT (Georgia Department of Transportation). (2013). Drilled Caisson Foundations. GDOT SSP 524. Atlanta, GA: GDOT.

6. Concrete Pumping (1999). Virginia Highway Project Boasts One of the Country's Biggest Bridges October 1999, <http://concretepumping.com/dictionary/virginia-highway-project-boasts-one-of-the-countrys-biggest-bridges-october-1999> (Accessed 10 October 2021).

7. Rau, E. and Goodyear, D. (2018). Portland's Sellwood Bridge, <https://www.structuremag.org/?p=13820> (Accessed 10 November 2021).

8. Overman, T. and Duerr, C. (2019). Reconstruction of the Historic BNSF Br. 482.1, <https://lpe.ku.edu/sites/kupce.ku.edu/files/docs/cpep/structural/speaker-presentations-2019/BNSFMemphisBridgeReconstruction.pdf> (Accessed 10 November 2021).

9. Singh, P. R. and Rai, D. C. (2018). "Effect of piped water cooling on thermal stress in mass concrete at early ages." J. Eng. Mech., 144(3): 04017183. doi: 10.1061/(ASCE) EM.1943-7889.0001418.

10. Yikici, T. A. (2015). "Evaluating Thermal Behavior and Use of Maturity Method in Mass Concrete." *Graduate Theses, Dissertations, and Problem Reports*. 7007.

11. Mehta, P.K. and Monteiro, P. J. M. (2006). Concrete: Microstructure, Properties, and Materials. 3rd Edition. New York, NY: The McGraw-Hill Companies, Inc.

12. ACI Committee 207. (2005). Guide to Mass Concrete (ACI 207.1R-05). Farmington Hill, MI: American Concrete Institute.

13. ACI Committee 207. (2007). Report on Thermal and Volume Change Effects on Cracking of Mass Concrete (ACI 207.2R-07). Farmington Hill, MI: American Concrete Institute.

14. Mindess, S., Young, J. F., and Darwin, D. (2003). Concrete. 2nd Edition. Upper Saddle River, NJ: Prentice-Hall.